This is a peer-reviewed, accepted author manuscript of the following article: Dai, Y., Qin, F., Liu, Y., Chen, H., & Berto, F. (2021). Characteristics and implications of material mismatch on mode II creep crack tip field: theoretical analysis and numerical investigation. Theoretical and Applied Fracture Mechanics, 114, [103035]. https://doi.org/10.1016/j.tafmec.2021.103035

Characteristics and implications of material mismatch on mode II creep crack tip field: Theoretical analysis and numerical investigation

Yanwei Dai[1]

Institute of Electronics Packaging Technology and Reliability, Faculty of Materials and Manufacturing, Beijing University of Technology, Beijing 100124, China

Beijing Key Laboratory of Advanced Manufacturing Technology, Beijing University of Technology, Beijing 100124, China

ywdai@bjut.edu.cn

Fei Qin

Institute of Electronics Packaging Technology and Reliability, Faculty of Materials and Manufacturing, Beijing University of Technology, Beijing 100124, China

Beijing Key Laboratory of Advanced Manufacturing Technology, Beijing University of Technology, Beijing 100124, China

Yinghua Liu

Department of Engineering Mechanics, AML, Tsinghua University, Beijing 100084, China

Haofeng Chen

Department of Mechanical & Aerospace Engineering, University of Strathclyde, Glasgow G1 1XJ, UK

Filippo Berto

NTNU, Department of Engineering Design and Materials, Richard Birkelands vei 2b, 7491 Trondheim, Norway

[1] Corresponding author: ywdai@bjut.edu.cn

Abstract

The mismatch effect in weldment is widely to be found in engineering practices. In this paper, the material mismatch effect on the mode II creep crack tip field is investigated and discussed. The mismatch effect on the $C(t)$-integral is presented. Both the local mismatch and the general mismatch are found to play important role in the $C(t)$-integral under mode II condition. The mismatch effect on the stress field of mode II creep crack is also studied. The two-order term solutions are adopted to characterize the material mismatch effect on the mode II creep crack. The effect of creep coefficient, creep exponent as well as the HAZ thickness on the high order term solutions are also presented. Some typical cases by considering general mismatch and local mismatch effect are given to make a comparisons between the HRR field, FE solutions and the two-order term solutions. It can be seen that the two-order term solutions can coincide with the full field FE solutions quite reasonably regardless of creep extent, creep exponent, mismatch factor, and HAZ thickness. The material mismatch effect on the high order term solutions is significant under some conditions. A theoretical formula is presented to show the implication of material mismatch effect on creep crack growth under mode II condition based on stress damage model.

Keywords: Mismatch effect; Mode II crack; Creeping solids; Two-order term solutions; Numerical analysis

1 Introduction

The material mismatch effect on the crack tip field in welded creeping materials at elevated temperature has been investigated widely in recent years [1, 2] as the high-temperature performance of these welded components is always limited by the creep failure of weldment [3], e.g. the cracking behavior always occurs in the heated affected zone (HAZ) [4]. Meanwhile, the already evidences found that it can affect the creep crack growth remarkably under some conditions [5-7]. A review on fracture and propagation of crack in weldment was presented by Zerbst et al. [8].

The material mismatch phenomenon, which is generally defined as the mismatch effect caused by the difference of material properties, is very common to be seen in many kinds of weldment in engineering practices. The effect of material mismatch can influence the crack tip field remarkably as it can cause the variations of the stress-strain field across the mismatched region. Hence, mismatch effect on crack tip can heighten or weaken the amplitude of the crack tip field or affect the so-called "constraint effect". Due to the important role of the material mismatch, the mismatch effect has been widely discussed in various backgrounds, e.g. elastic materials [9-12], elastoplastic materials [13-17] and, more recently, the creeping materials [18-24].

A wide range of topics related with material mismatch effect have been investigated, e.g. the mismatch effect on the crack driving forces such as stress intensity factor [12] , J-integral [25, 26] and $C(t)$-integral [27, 28], constraint effect [29, 30], crack initiation [30, 32], and crack growth estimation [30-33]. However, it should be mentioned that the above mentioned researches are mainly for mode I or interface condition. There are a few of discussions on mode II type creep crack. Among those, Poquillon et al. [34] presented an experimental studies on mode II creep crack tip field. The earlier work given by Brockenbrough et al. [35] shows that extension of the creep zone of mode II is faster than that of mode I. In recently, the high order term asymptotic solutions for mode II creep crack under homogeneous condition were reported by Dai et al. [36, 37]. However, there is no investigation on the mismatch effect of the mode II creep crack

tip field in the available literatures as far as the authors' knowledge. What's more, the behavior and the role of the mismatch effect on the mode II creep crack tip field cannot be understood clearly before it is studied.

Based on the aforementioned reviews, it can be found: (1) the definition of the "mismatch factor" in various kinds of materials are different, e.g. the difference of elastic modulus is defined for elastic mismatch, the difference of strength is always defined for plastic mismatch, and the difference of creep constant is defined as creep mismatch; (2) the effect of material mismatch may be dependent on the structure geometry, e.g. HAZ thickness; (3) the material mismatch may lead to the change of the constraint effect level of a crack front. It implies that the influence of the material mismatch on the creep crack front could be a consequence of comprehensive effects.

The aim of this paper is to investigate the material mismatch effect on the mode II creep crack front under plane strain condition. With employing the numerical and analytical investigations on the mode II creep crack by considering the material mismatch effect, the effect of welded material and geometry is presented. The organization of this paper is as follows. The theoretical background on mismatch effect and the crack front field of mode II creep crack are given in Section 2. The finite element procedures are illustrated in Section 3. The results and discussions are presented in Section 4. The higher order term effect on creep crack growth and creep toughness considering material mismatch effect will be discussed in Section 5. The conclusions are drawn in the last section.

2 Theoretical background

A power-law creeping material under multiaxial state, i.e. Norton's constitutive equation, in this paper is adopted as [38]

$$\dot{\varepsilon}_{ij} = \frac{1+\nu}{E}\dot{S}_{ij} + \frac{1-2\nu}{3E}\dot{\sigma}_{kk}\delta_{ij} + \frac{3}{2}\dot{\varepsilon}_0\left(\frac{\sigma_e}{\sigma_0}\right)^{n-1}\frac{S_{ij}}{\sigma_0} \tag{1}$$

$$S_{ij} = \sigma_{ij} - \sigma_{kk}\delta_{ij}/3 \tag{2}$$

$$\sigma_e^2 = \frac{3}{2} S_{ij} S_{ij} \tag{3}$$

where E, n, $\dot{\sigma}$, $\dot{\varepsilon}_0$, σ_0 v and δ_{ij} are the Young's modulus, creep exponent, stress rate, reference creep strain rate, reference stress, Poisson's ratio and Kronecker delta, respectively. S_{ij} and σ_e are the deviatoric stress and Mises equivalent stress, respectively. As usual, the creep coefficient $B = \dot{\varepsilon}_0 / \sigma_0^n$. For two-dimensional conditions under polar coordinate, the subscript i, j take r and θ, respectively. The polar coordinate used here is presented in Fig. 1.

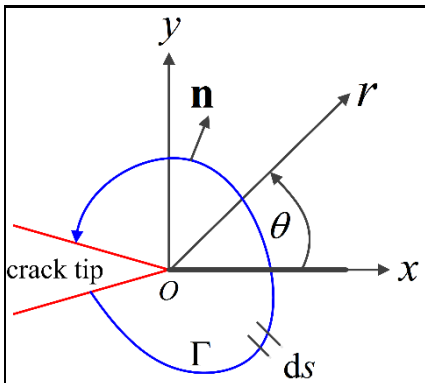

Fig. 1 Configuration of the polar coordinate system of a crack tip field

According to Dai et al. [36], the two-termed stress field for a mode II creep crack tip in a homogeneous material can be written as:

$$\frac{\sigma_{ij}(r,\theta,t)}{\sigma_0} = A_1(t)\bar{r}^{s_1}\tilde{\sigma}_{ij}^{(1)}(\theta) + A_2(t)\bar{r}^{s_2}\tilde{\sigma}_{ij}^{(2)}(\theta) \tag{4}$$

in which $A_i(t)$ $(i=1,2)$ are the i-th undetermined constants as a function of creep time and subscript i represents the i-th term, respectively. $\tilde{\sigma}_{ij}^{(i)}(\theta)$ is the dimensionless angular function corresponding to the i-th term which has been given in [36]. As an example, the angular distribution functions for n=7 are given in Appendix A. s_i is the power exponent for the i-th term. $\bar{r} = r/L$ and L here is a characteristic length. Herein, L can be selected as any number, e.g. minimum element size, plate thickness, crack length, even unity. It should be noted that the value of L dose not affect the values of $A_1(t)$-term as the role of characteristic length L is only for the aim of dimensionless

treatment, which will not affect the solutions.

The first term $A_1(t)$ with the HRR singularity is expressed as

$$A_1(t)=\left(\frac{C(t)}{\dot{\varepsilon}_0\sigma_0 I_n L}\right)^{1/(n+1)} \tag{5}$$

where $C(t)$ is the $C(t)$-integral and I_n is the integration constant which is demonstrated to be the same as the I_n tabled by Symington et al. [39], and it also depends on crack front stress state. The definition of $C(t)$-integral is written as [40]

$$C(t)=\int_{\Gamma\to 0} W^* \mathrm{d}y - T_i\left(\frac{\partial \dot{u}_i}{\partial x}\right)\mathrm{d}s \tag{6}$$

where Γ is a counterclockwise integration contour around the crack tip as shown in Fig. 1, T_i, $\dot{u}_i$, $\mathrm{d}y$ and $\mathrm{d}s$ are the traction vector on Γ, the displacement rate, the increments in y-direction and along Γ, respectively. The C^* will replace $C(t)$ as if the creep extent is under extensive range and presents to be path-independent. The determination of the second order term $A_2(t)$ can be seen in Dai et al. [36] which is dependent on the creep exponent n.

The stress components with a bar over quantities below which takes the effect of material mismatch into account and can be rewritten as:

$$\frac{\hat{\sigma}_{ij}(r,\theta,t)}{\sigma_0}=\hat{A}_1(t)\bar{r}^{s_1}\tilde{\sigma}_{ij}^{(1)}(\theta)+\hat{A}_2(t)\bar{r}^{s_2}\tilde{\sigma}_{ij}^{(2)}(\theta) \tag{7}$$

in which all the quantities in Eq. (7) have the same meaning as those in Eq. (4). Note that the selection of the material constant, i.e. $\dot{\varepsilon}_0$ and σ_0, in $\hat{A}_1(t)$-term will be discussed in Section 4.

In order to characterize the stress distributions ahead of mode II creep crack, the redistribution time, which is directly extended from mode I, is always adopted as below:

$$t_{\mathrm{red}}=\frac{(1-\nu^2)K_{\mathrm{II}}^2}{EC^*} \tag{8}$$

where K_{II} is the mode II stress intensity factor.

3 Numerical procedures

As there is no standard tested specimen for mode II type crack, the compact tension shear (CTS) specimen is adopted to simulate the pure mode II deformation as the CTS specimen has been used widely in other researchers' investigations [41-44] for mode II or mixed crack. The configuration and FE meshes for the whole geometry and crack are shown in Fig. 2. The specific geometry of the specimen is similar to that used in Roy et al. [42] where the width and height of the CTS specimen are 90 mm and 148 mm, respectively. The radius of the outer boundary for the fixture is 130 mm. The width of heated affected zone (HAZ) is denoted as h. The crack is generally assumed to be in the center of HAZ. The crack length denoted in Fig. 2 is a, and a/W is equal to 0.5 in this paper if it is not extra stated. The fixture and the specimen are treated to be in one piece and the fixture is considered to be rigidity. The diameter of the loading hole is 10 mm.

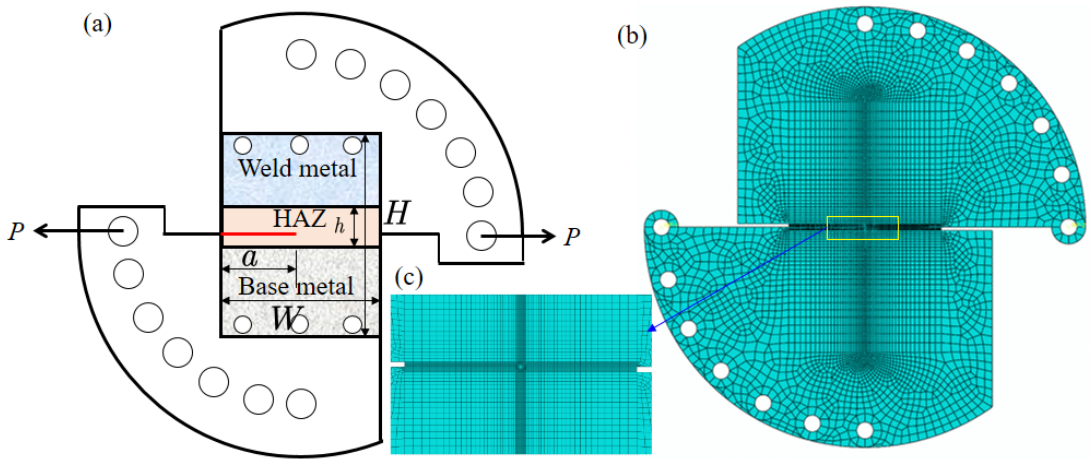

Fig. 2 Geometry configuration and FE meshes: (a) Specimen geometry; (b) FE meshes; (c) Crack tip meshes

The FE code ABAQUS is adopted to perform the numerical analysis. To avoid the shear locking, the hybrid 8-node plane strain elements with full integration (CPE8H) is adopted. The total number of elements used in calculations are between 10058 and 10471. The singular element is adopted for the first ring mesh ahead of crack tip and the mesh is deemed to be refined as the SIF for the crack tip is not changed with the

increase of element number. As the computed SIF shows that the mode I SIF is far more less than mode II SIF which implies that the crack tip can be treated to be the pure mode II case. On the $C(t)$-integral, the values of $C(t)$-integral are extracted from ABAQUS directly with contour integration. C^*-integral will be obtained when the creep is under extensive state. During the computations, the linearly elastic properties, e.g. Young's modulus and Poisson's ratio, are kept to be 175 GPa and 0.3, respectively. Nine typical cases, shown in Table 1 numbered from C1 to C9, are selected to study the material mismatch effect with a fixed creep exponent of n=7. The data in Table 1 is available from [45].

Table 1 Material constants used in the computations

n	B_w/B_b	B_{HAZ}/B_b	B_b	B_w	B_{HAZ}	MF_W	MF_{HAZ}	No
7	5	6	3.2E-19	1.60E-18	1.92E-18	0.79	0.77	C1
7	5	1.2	3.2E-19	1.6E-18	3.84E-19	0.79	0.97	C2
7	5	0.167	3.2E-19	1.6E-18	5.34E-20	0.79	1.29	C3
7	0.2	6	3.2E-19	6.4E-20	1.92E-18	1.26	0.77	C4
7	0.2	1.2	3.2E-19	6.4E-20	3.84E-19	1.26	0.97	C5
7	0.2	0.167	3.2E-19	6.4E-20	5.34E-20	1.26	1.29	C6
7	1	6	3.2E-19	3.2E-19	1.92E-18	1	0.77	C7
7	1	1	3.2E-19	3.2E-19	3.2E-19	1	1	C8
7	1	0.167	3.2E-19	3.2E-19	5.34E-20	1	1.29	C9

Among those data in Table 1, there are two kinds of mismatch effect which are characterized by the weld mismatch factor, MF_W, and the HAZ mismatch factor, MF_{HAZ}, respectively. The weld mismatch factor is defined as:

$$MF_w = \left(\frac{B_b}{B_w} \right)^{1/n} \tag{9}$$

Accordingly, the HAZ mismatch factor is given as

$$MF_{HAZ} = \left(\frac{B_b}{B_{HAZ}} \right)^{1/n} \tag{10}$$

where B_b, B_{HAZ} and B_w are the creep coefficient of the base metal, HAZ metal and weld metal, respectively. The weld mismatch factor and HAZ mismatch factor are defined to characterize the *general mismatch* condition and *local mismatch* condition, respectively. Regardless of general mismatch or local mismatch, the overmatch

represents that the mismatch factor is greater than 1, however, the undermatch is defined as the mismatch factor is less than 1. The evenmatch condition, i.e. the homogeneous case, is approached when mismatch factor is identical to 1. The nine cases can be categorized to be three conditions, e.g. the Condition A contains C1, C2 and C3, the Condition B contains C4, C5 and C6, and the other three cases are the Condition C. The Condition A represents the general mismatch factor is 0.79, i.e. undermatch condition, while the local mismatch factor varies from 0.77 to 1.29 which cover the undermatch and overmatch cases. The Condition B means that the general mismatch factor is 1.26, i.e. overmatch condition, while the local mismatch factor is similar to that of Condition C. The general mismatch factor for Condition C is set to be 1, evenmatch condition and the three local mismatch factors also varies from 0.77 to 1.29. C8 in Condition C indicates that there is no mismatch effect for both general mismatch and local mismatch for C8.

4 Results and discussions

4.1 Mismatch effect on $C(t)$-integral

To illustrate the mismatch effect on the C^*-integral, the variation of C^*-integral with mismatch factor is shown in Fig. 4. The results are obtained from the FE calculations for CTS specimens with a/W=0.5 under shearing loading of 600 N with K_{II}=40.1 $\mathrm{MPa}\bullet\mathrm{mm}^{0.5}$ for all the analyzed cases. It can be found that the mismatch effect on the creep crack tip field can affect the $C(t)$-integral greatly, and the values of C^* at the extensive creep under different mismatch factors and h are totally different.

It can be seen that the C^*-integral is affected by both the general mismatch and the local mismatch. The C^*-integral decreases with the increase of MF_{HAZ} regardless of MF_{W} and h. The C^*-integral also decreases with the rise of MF_{W} at fixed MF_{HAZ}. In general, the C^*-integral is larger than the C^*-integral of homogeneous case for

$MF_{\mathrm{HAZ}}<1$ and smaller than the C^*-integral of homogeneous case for $MF_{\mathrm{HAZ}}>1$. It implies that the effect of the material property in HAZ plays significant role in the weldment.

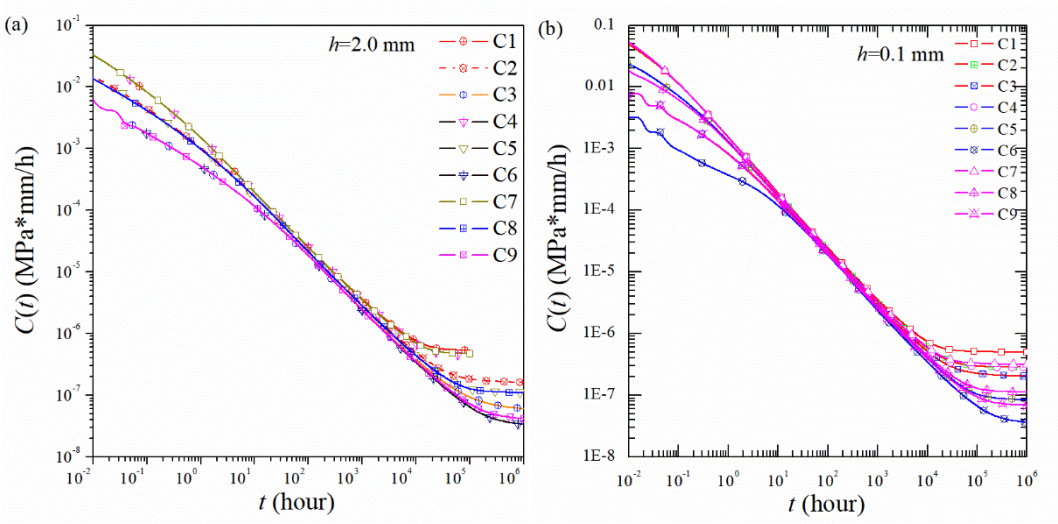

Fig. 3 Variations of $C(t)$ with creep time: (a) h = 2 mm; (b) h = 0.1 mm

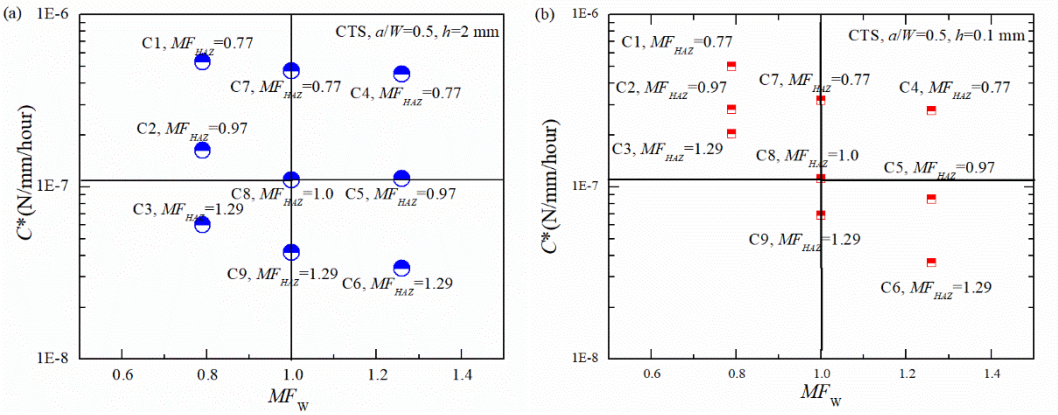

Fig. 4 Variations of C^* with general mismatch factors: (a) h = 2 mm; (b) h = 0.1 mm

Table 2 Ratio of C^* between mismatched case and homogeneous case

	Condition A			Condition B			Condition C		
MF_{W}=	0.79	0.79	0.79	1.26	1.26	1.26	1.00	1.00	1.00
MF_{HAZ}=	0.77	0.97	1.29	0.77	0.97	1.29	0.77	1.00	1.29
h=2 mm	4.8429	1.4818	0.5516	4.1254	1.0196	0.3076	4.2838	1	0.3794
h=0.1mm	4.4534	2.5216	1.8149	2.4727	0.7531	0.3233	2.8245	1	0.6105

From Table 2, the ratio of C^* between mismatch and homogeneous case are shown clearly. It can be seen that the values with $MF_{\mathrm{HAZ}}<1$ are all larger than 1 which reveals that the mismatch effect under this condition can enhance the C^*-integral of the mode

II creep crack tip. On the contrary, the ratio with $MF_{\mathrm{HAZ}}>1$ are generally less than 1 which means that the mismatch effect under this condition can weaken the C^*-integral.

According to Riedel [46], the $C(t)/C^*$ relation is written as

$$\frac{C(t)}{C^*}=1+\frac{t_{\mathrm{red}}}{(n+1)t} \tag{11}$$

in which t_{red} is the redistribution time defined in Eq. (8). Originally, Eq. (11) is applied for the mode I crack tip field only. However, the relation can be still available to be used under mode II case according to our recent reports [43, 44]. For the mismatch condition discussed in this paper, as the creep crack tip still holds HRR singularity. Thereafter, Eq. (11) can be extended to mode II case directly. The normalized $C(t)/C^*$ relation shown in Fig. 5 also verifies this point. It has been shown clearly that the FE solutions agree quite well with Eq. (11) except in the region of $t/t_{\mathrm{red}}<1$. Generally, the FE results for $C(t)/C^*$ relation under different mismatch factors coincide with each other perfectly regardless of mismatch conditions.

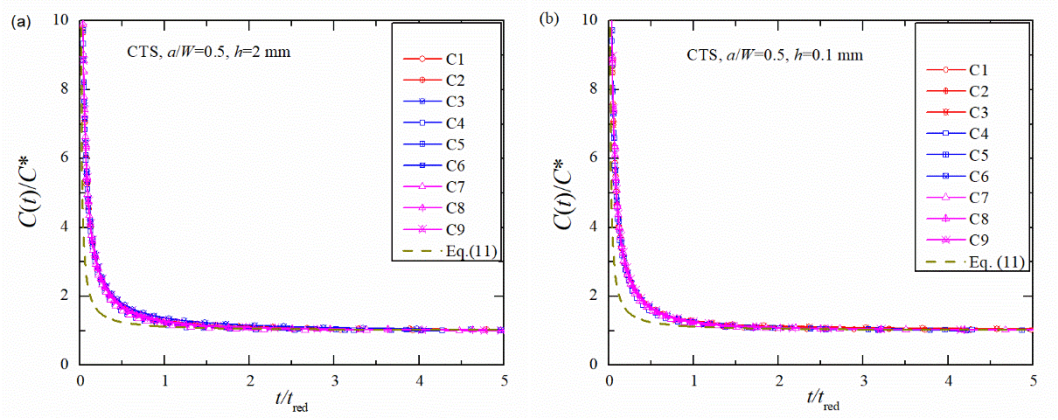

Fig. 5 Variation of $C(t)/C^*$ with the normalized time t/t_{red}: (a) h =2 mm and (b) h =0.1 mm

4.2 Mismatch effect on the stress field

The radial stress distributions along $\theta=0^{\circ}$ and 30° for different mismatch factors under shear loading with 600 N at the creep time of 1000000 hours are presented in Fig.

6. The creep time adopted here is to keep the crack tip under extensive range. The $C(t)$-integral under this situation has been given in Section 4.1 where $C(t)$-integral under different conditions have been presented. It can be seen from Fig. 6 (a) clearly that cases C3, C9 and C6 hold higher radial shearing stress distributions among those given solutions. The shearing stress components for C1, C4 and C7 are lower than the homogeneous case. For C2, C5 and C8, those values are slight higher than homogeneous case. Considering the material constants of these cases, the lower creep coefficient will lead to the higher stress components. Similar tendencies can be found in Fig. 6(d) for shearing stress components along $\theta = 30^{o}$. For tangential stress and radial stress distributions, the tendencies presented to be reversed as the values are negative. Compared with the HRR solutions which computed with evenmatch creep constants, the FE solutions in C8 are quite close to HRR solutions.

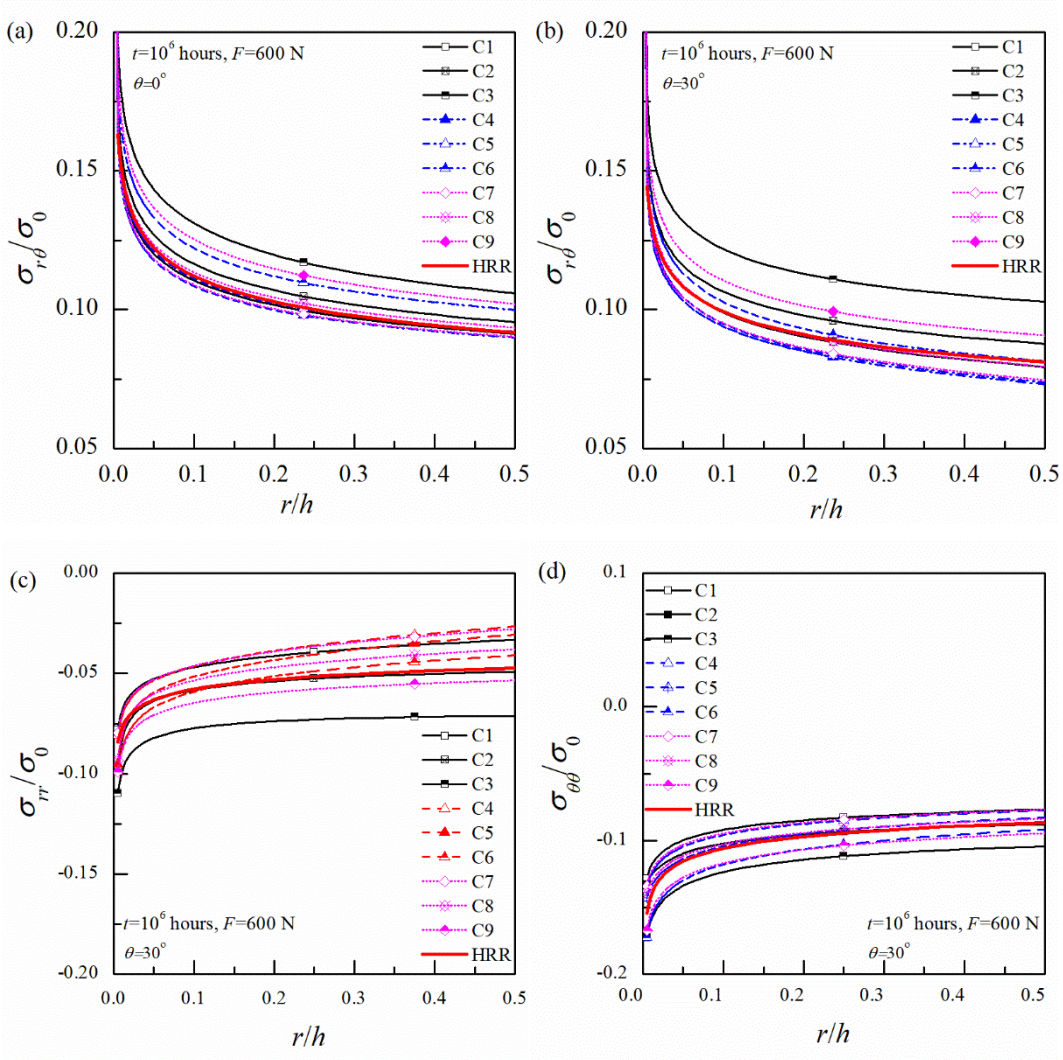

Fig. 6 Comparisons of the stress components between HRR solution and FE solutions under different mismatch factors for HAZ width h = 2 mm in radial direction: (a) $\sigma_{r\theta}$ at θ= 0°; (b) $\sigma_{r\theta}$ at θ=30°; (c) σ_{rr} at θ= 30°; (d) $\sigma_{\theta\theta}$ at θ= 30°

According to the previous investigation [37], results show that the analytical HRR solutions calculated with material constants of HAZ metal approach to the FE solutions quite closely regardless of various conditions, but deviates from HRR solutions computed with material constants of base metal greatly. It implies that the first order stress field under mismatch conditions for h = 2 mm can be presented to be a reference field which should be written as below [37]:

$$\frac{\hat{\sigma}_{ij}(r,\theta,t)}{\sigma_0^{\text{tip}}}=\left(\frac{C(t)}{\dot{\varepsilon}_0^{\text{tip}}\sigma_0^{\text{tip}}I_n^{\text{tip}}L}\right)^{1/(n+1)}\bar{r}^{s_1}\tilde{\sigma}_{ij}^{(1)}(\theta) \tag{12}$$

in which $\dot{\varepsilon}_0^{\text{tip}}$, σ_0^{tip} and I_n^{tip} are the reference strain rate, reference stress and integration constant where the crack tip locates. Comparisons of the stress components in radial direction under different mismatch factors for h = 0.1 mm are given in Fig. 7. It can be found that the radial stress distribution tendencies are quite similar to the condition of h = 2.0 mm.

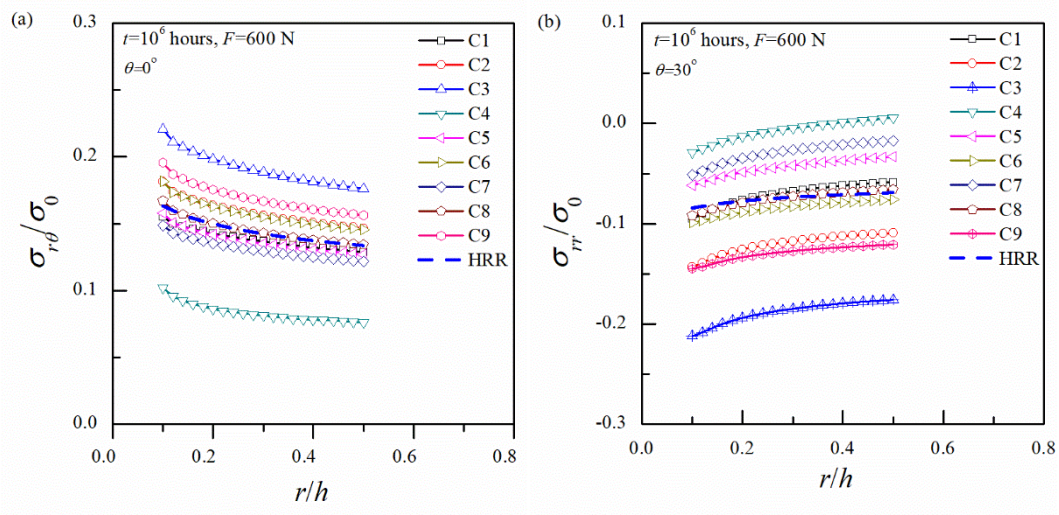

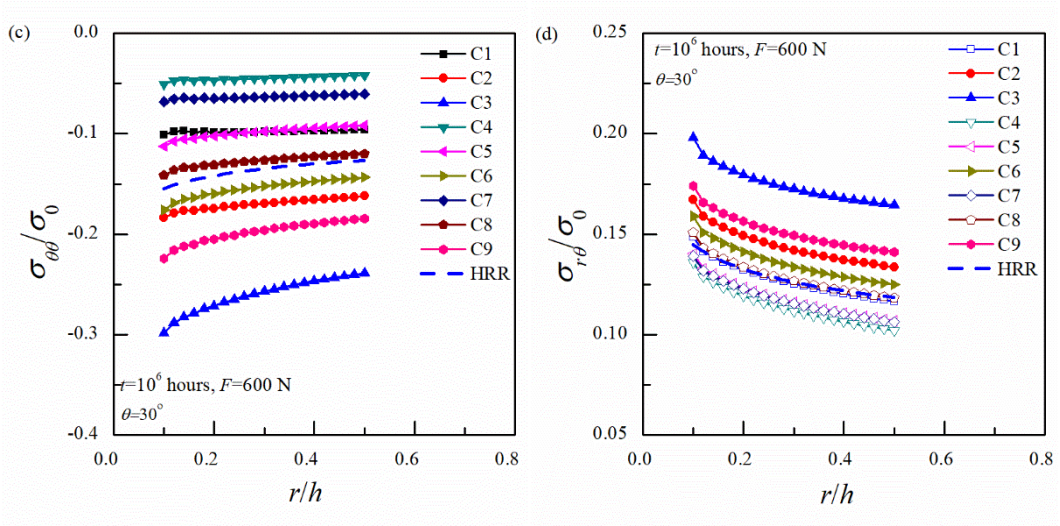

Fig. 7 Comparisons of the stress components between HRR solution and FE solutions under different mismatch factors for HAZ width h = 0.1 mm in radial direction: (a) $\sigma_{r\theta}$ at θ= 0°; (b) $\sigma_{r\theta}$ at θ=30°; (c) σ_{rr} at θ= 30°; (d) $\sigma_{\theta\theta}$ at θ= 30°

4.3 Mismatch effect on the higher order terms

According to the previous illustrations, the stress field is significantly affected by the material mismatch effect. Some investigations have demonstrated that the material mismatch can cause the variation of the constraint level. Hence, it is meaningful to study the material mismatch effect on the second order term of mode II creep crack tip field. The material mismatch effect on the mode II creep crack will be discussed in the following.

4.3.1 Condition A: General undermatch condition

The so-called general undermatch condition represents Condition A which is defined in Table 2, i.e. C1, C2 and C3 with MF_{HAZ} = 0.77, 0.97 and 1.29, are included under this condition which will be discussed in this section.

According to Eq. (7) and Eq. (12), the two-order termed solutions for mode II creep crack considering material mismatch effect can be presented as:

$$\frac{\hat{\sigma}_{ij}(r,\theta,t)}{\sigma_0^{\mathrm{tip}}}=\left(\frac{C(t)}{\dot{\varepsilon}_0^{\mathrm{tip}}\sigma_0^{\mathrm{tip}}I_n^{\mathrm{tip}}L}\right)^{1/(n+1)}\bar{r}^{s_1}\tilde{\sigma}_{ij}^{(1)}(\theta)+\hat{A}_2(t)\bar{r}^{s_2}\tilde{\sigma}_{ij}^{(2)}(\theta) \tag{13}$$

Note that σ_0^{tip} is the reference stress of the material where the creep crack tip locates. Herein, the creep crack tip locates at the HAZ in this investigation. Hence, the reference stress σ_0^{tip} always adopts the reference stress of material in HAZ. The point match technique [47] can be used to determine $\hat{A}_2(t)$.

The angular distributions for C1, C2 and C3 by comparing HRR solutions, two-order term solutions, FE results and the FE results of homogeneous case at the fixed distance of 0.1 mm are shown in Fig. 8, respectively. It should be noted that the HRR solutions are calculated with Eq. (12), i.e. the material constants adopt these material constants where the crack tip locates. The $C(t)$-integral are the same as shown in Section 4.1 and these FE solutions are extracted at the creep time of 10^6 hours. Among these solutions, the value of $\hat{A}_2(t)$ for C1 at 0.1 mm and 1 mm at this calculated creep time are 0.144 and 0.0177, respectively. The value of $\hat{A}_2(t)$ for C2 at 0.1 mm and 1 mm at this calculated creep time are 0.125 and 0.00248, respectively. For C3, The value of $\hat{A}_2(t)$ at 0.1 mm and 1 mm at creep time of 10^6 hours are 0.123 and -0.0178. It implies that the second order term decreases with increase of MF_{HAZ}.

The interesting thing is that the deviations between HRR results and the FE solutions enlarge with the decrease of MF_{HAZ} where C3 presents that the most remarkable difference between HRR field and FE solutions. C1 shows the lowest remarkable difference between HRR field and FE solutions. It may imply that the undermatch of the local mismatch factor enlarges the deviations of the stress field between HRR field and full field. Due to the asymptotic nature, the deviation between the HRR field and FE solutions heightens at 1 mm compared with that of 0.1 mm. It can be also found that the most significant difference for tangential stresses occurs at around 75°-90°.

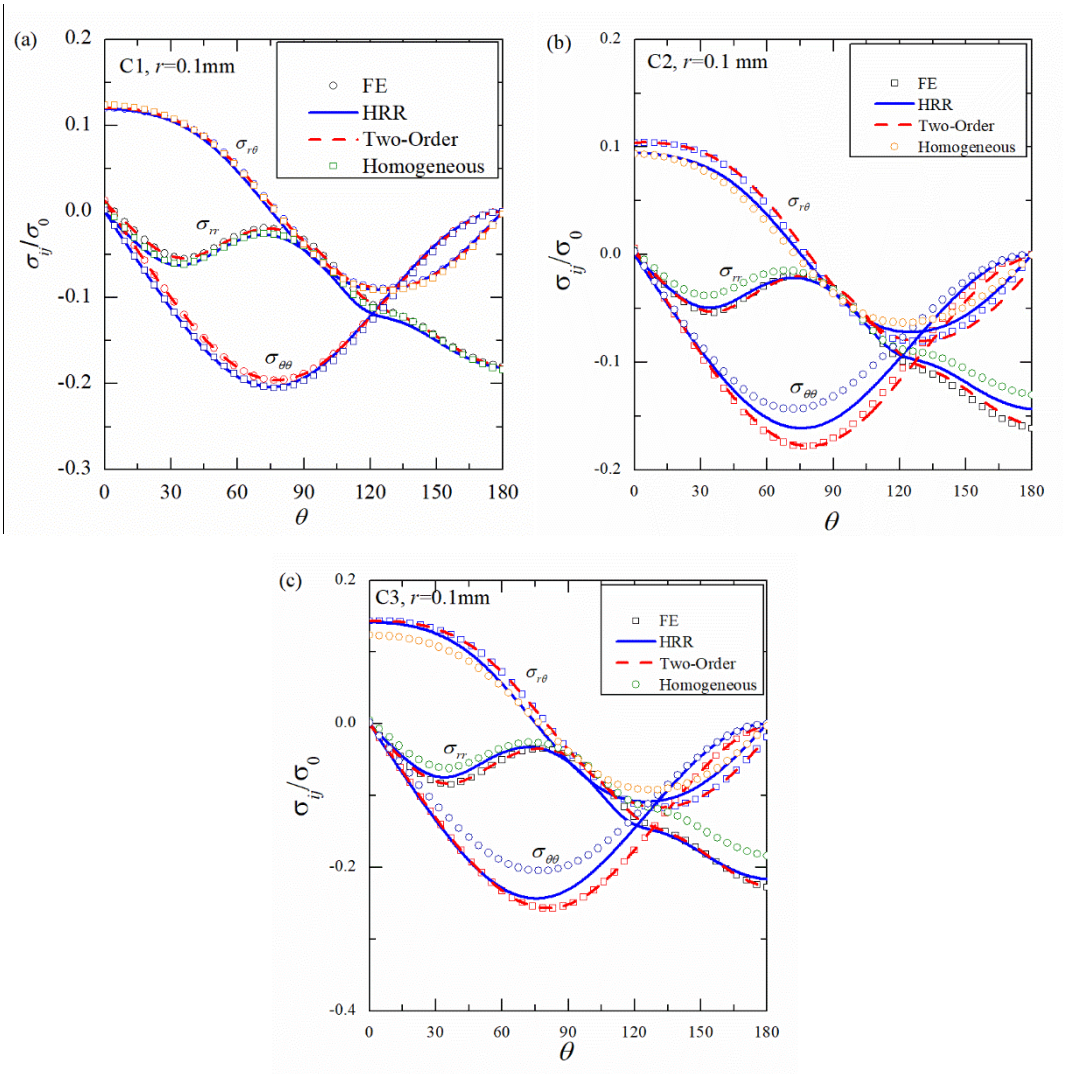

Fig. 8 Comparisons of angular stress distributions between FE, HRR and two-order term solutions at r=0.1 mm: (a) C1, (b) C2 and (c) C3

With the presented angular distributions, one can find that the most significant difference region between HRR field and FE solutions happens at around 75°-90°. To show the variation of the stress components in radial direction, the radial distributions for stresses of C1, C2 and C3 along 0° and 90° are presented in Fig. 9, Fig. 10 and Fig. 11, respectively. It can be found that the difference between stresses under FE calculations, HRR results and two-order termed solutions are quite small in direction of 0°. However, the difference between HRR field and FE results is remarkable in 0° though the two-order term solution can agree with the FE solutions very well. It should be pointed out that the FE solutions are much high than the HRR solutions for C1 but lower than that for C3.

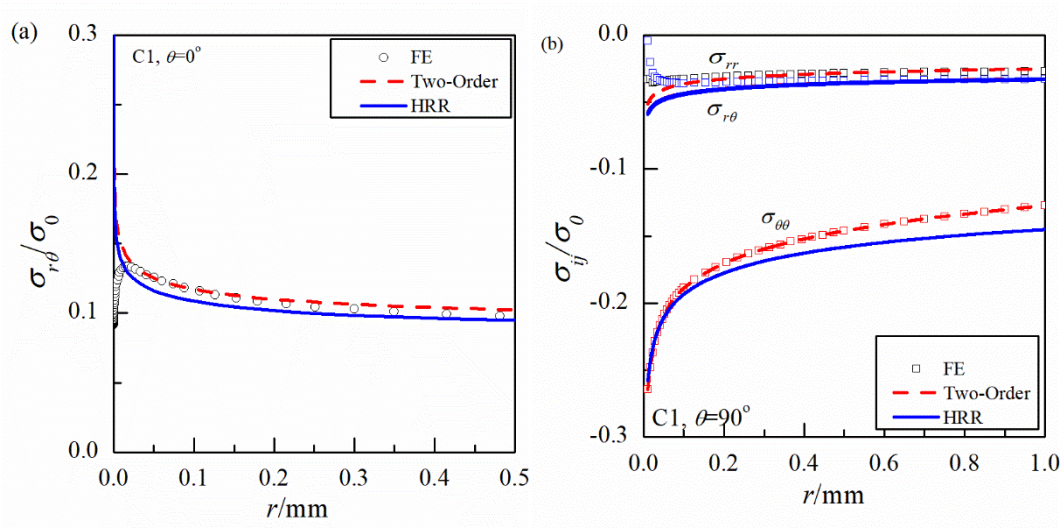

Fig. 9 Comparisons of radial stress distributions for C1 between FE, HRR and two-order term solutions along (a) 0° and (b) 90°

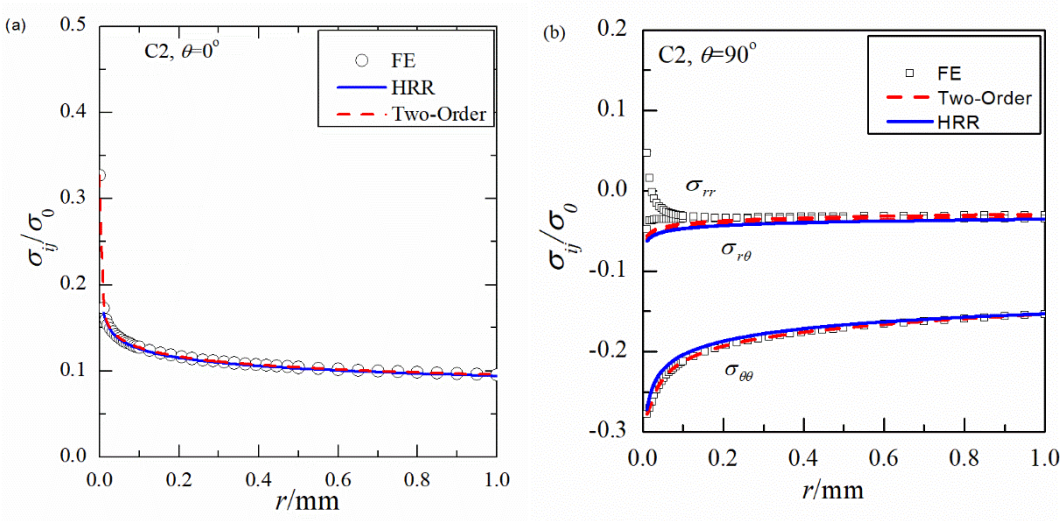

Fig. 10 Comparisons of radial stress distributions for C2 between FE, HRR and two-order term solutions along (a) 0° and (b) 90°

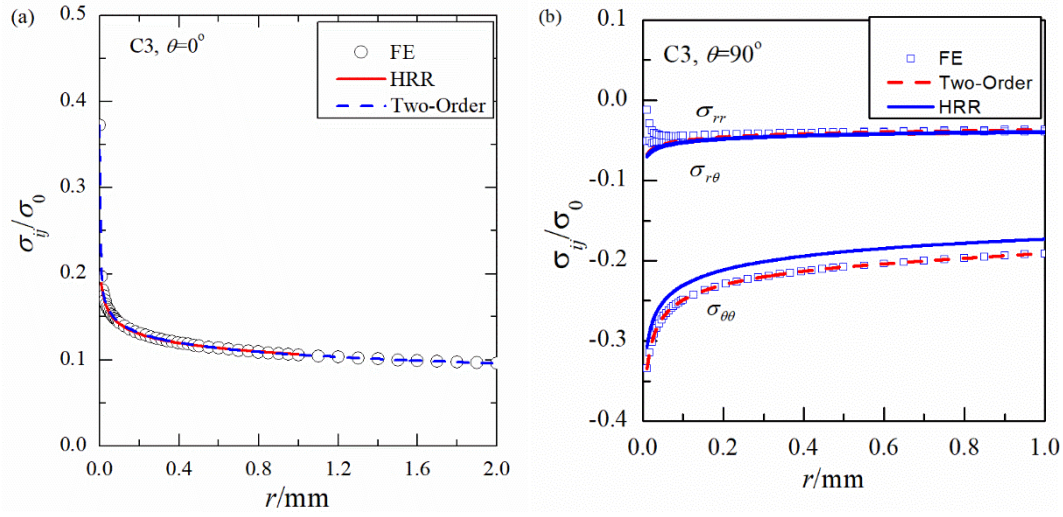

Fig. 11 Comparisons of radial stress distributions for C3 between FE, HRR and two-order term

solutions along (a) 0° and (b) 90°

4.3.2 Condition B: General overmatch condition

The angular distributions of stress components under general overmatch condition, i.e. $MF_w > 1$ with $MF_{HAZ} = 0.77$, 0.97 and 1.29, are shown in Fig. 12, respectively. It can be seen that the stress components under HRR field is lower than those of FE solutions and the deviations between HRR field and FE enlarges with the increase of distance from crack tip. Compared with the discrepancies for those general undermatch conditions, the differences between the HRR field and FE solutions are generally positive. The most significant occurs for C6 which presents to be the lowest creep coefficient. For C4 and C5, the deviations between HRR field and the mismatched FE creep crack tip field is not that remarkable.

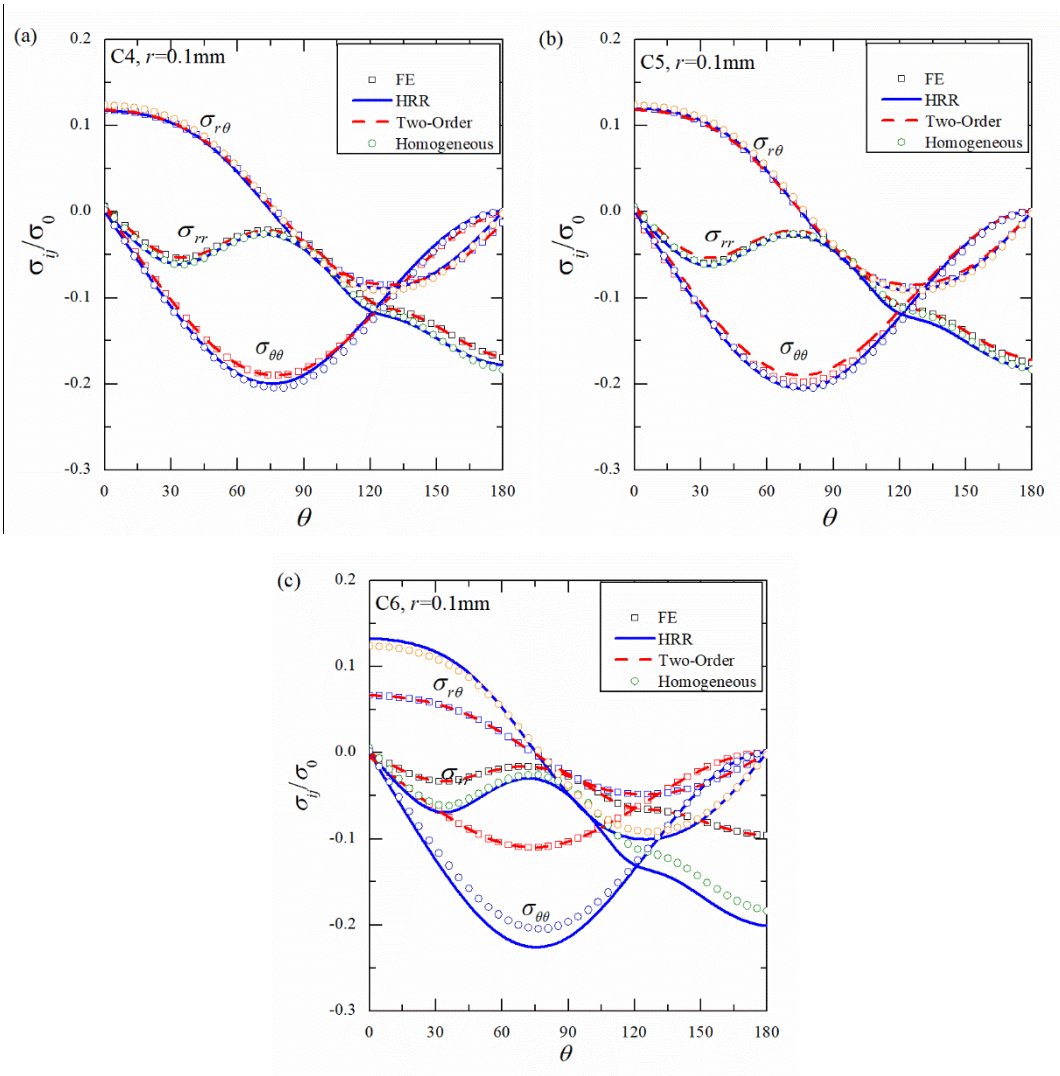

Fig. 12 Comparisons of angular stress distributions for C4, C5 and C6 between FE, HRR and Two-Order term solutions at r=0.1 mm: (a) C4; (b) C5; (c) C6

The radial distributions in 0° and 90° are presented in Fig. 13, Fig. 14 and Fig. 15, respectively. The shearing stresses with different local mismatch factors MF_{HAZ} presents that the HRR field is always smaller than those of FE solutions. However, the two-order term solutions can agree with the FE results very well regardless of the mismatch factors and the locations of the stresses. It also reveals that the mismatch effect under general overmatch condition heightens the full field to be higher than those of the FE field.

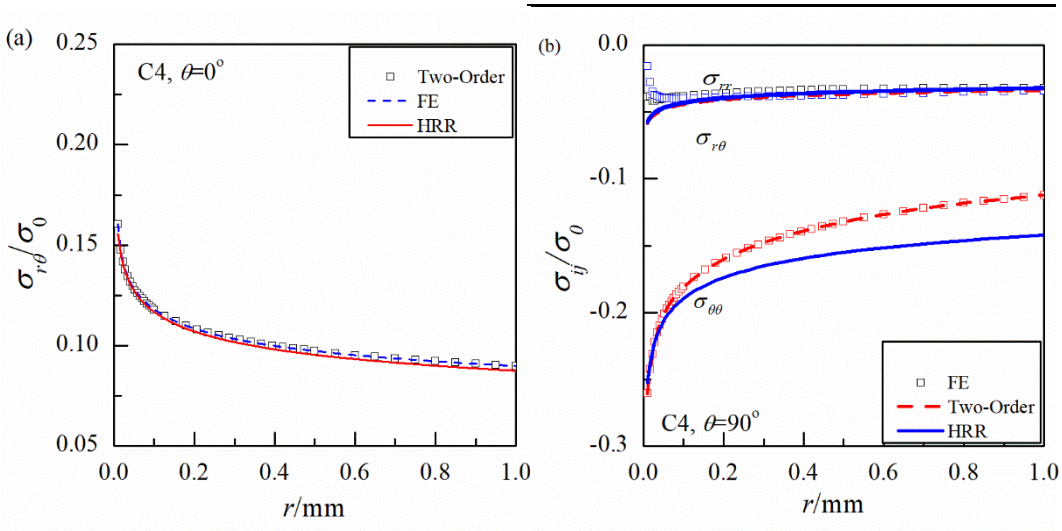

Fig. 13 Comparisons of radial stress distributions for C4 between FE, HRR and two-order term solutions along (a) 0° and (b) 90°

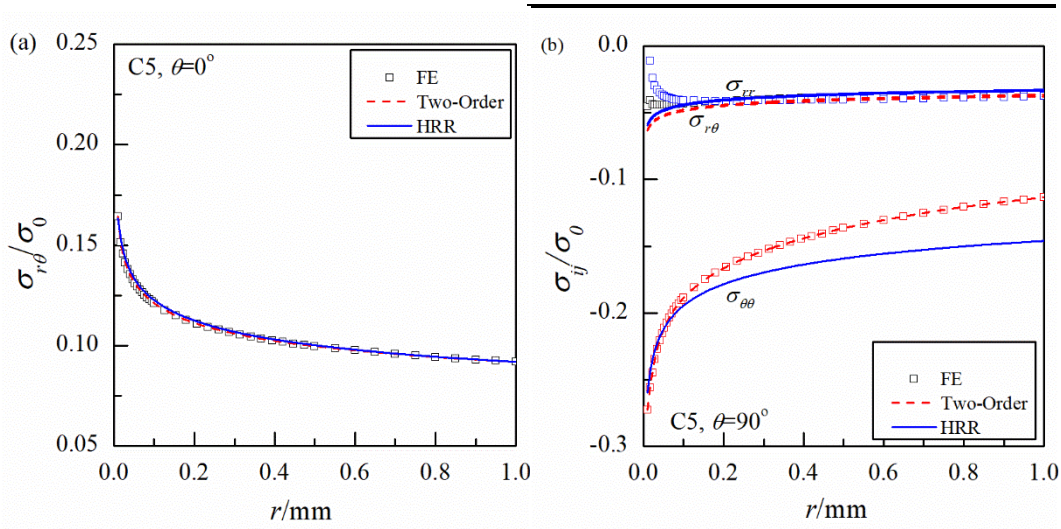

Fig. 14 Comparisons of radial stress distributions for C5 between FE, HRR and two-order term solutions along (a) 0° and (b) 90°

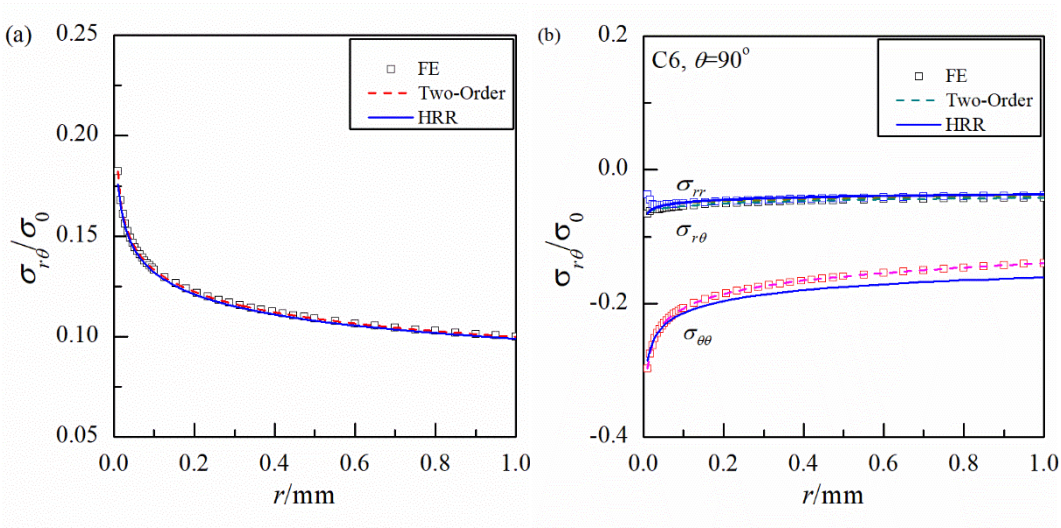

Fig. 15 Comparisons of radial stress distributions for C6 between FE, HRR and two-order term solutions along (a) 0° and (b) 90°

4.3.3 Condition C: General evenmatch condition

The angular stress distributions for C7, C8 and C9 are presented in Fig. 16 and radial distributions for C7, C8 and C9 are given in Fig. 17, Fig. 18 and Fig. 19, respectively. For the general evenmatch condition, the deviation between the HRR field and the FE solutions are less remarkable than those of undermatch and overmatch conditions.

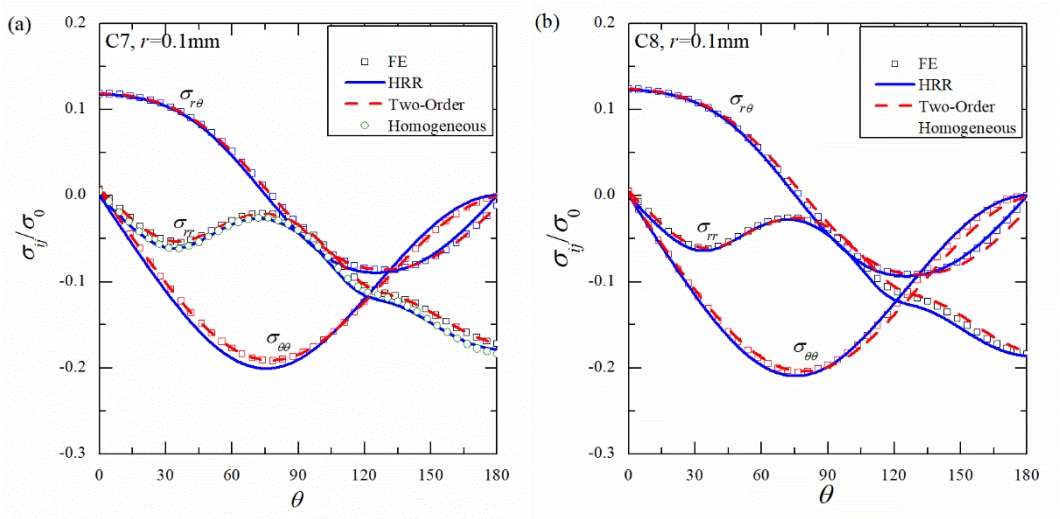

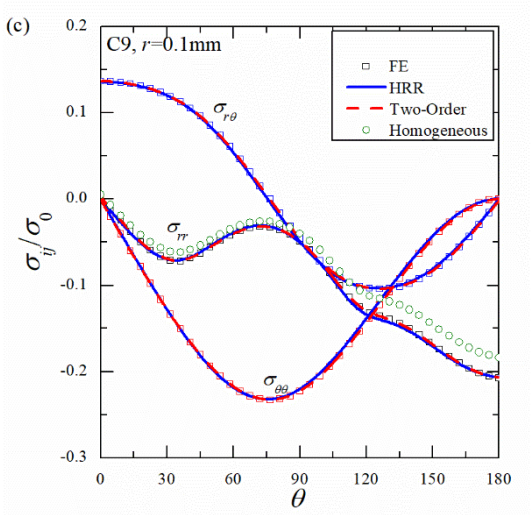

Fig. 16 Comparisons of angular stress distributions for C7, C8, C9 between FE, HRR and two-order term solutions at r=0.1 mm: (a) C7; (b) C8; (c) C9

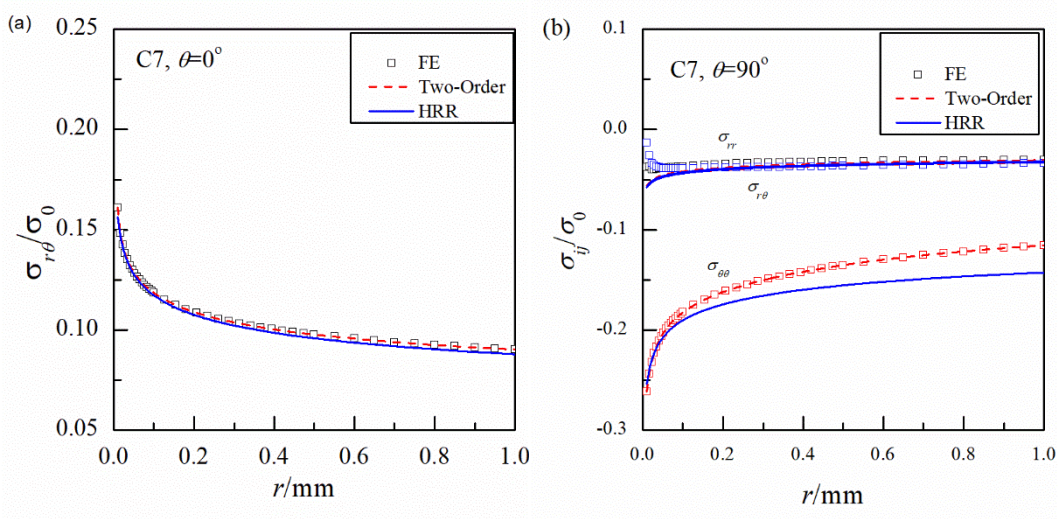

Fig. 17 Comparisons of radial stress distributions for C7 between FE, HRR and two-order term solutions along (a) 0° and (b) 90°

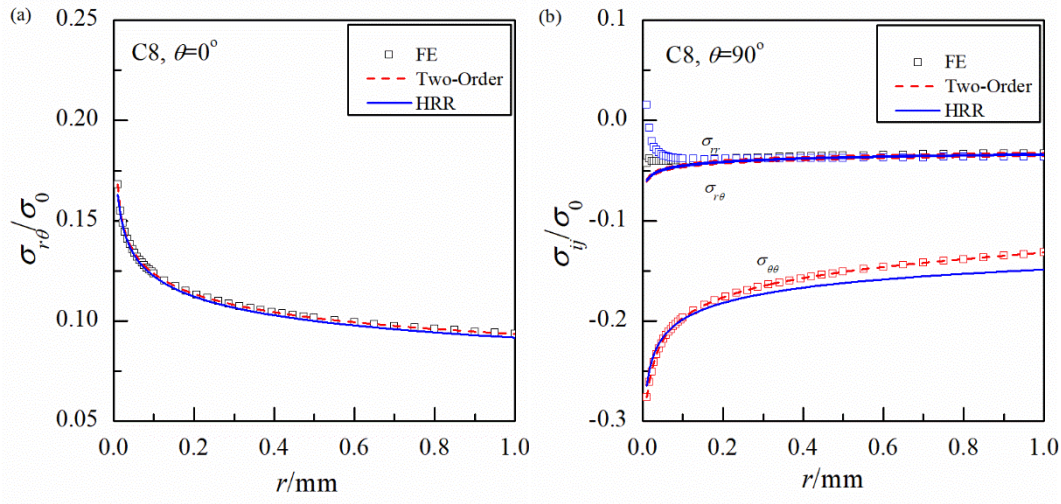

Fig. 18 Comparisons of radial stress distributions for C8 between FE, HRR and two-order term

solutions along (a) 0° and (b) 90°

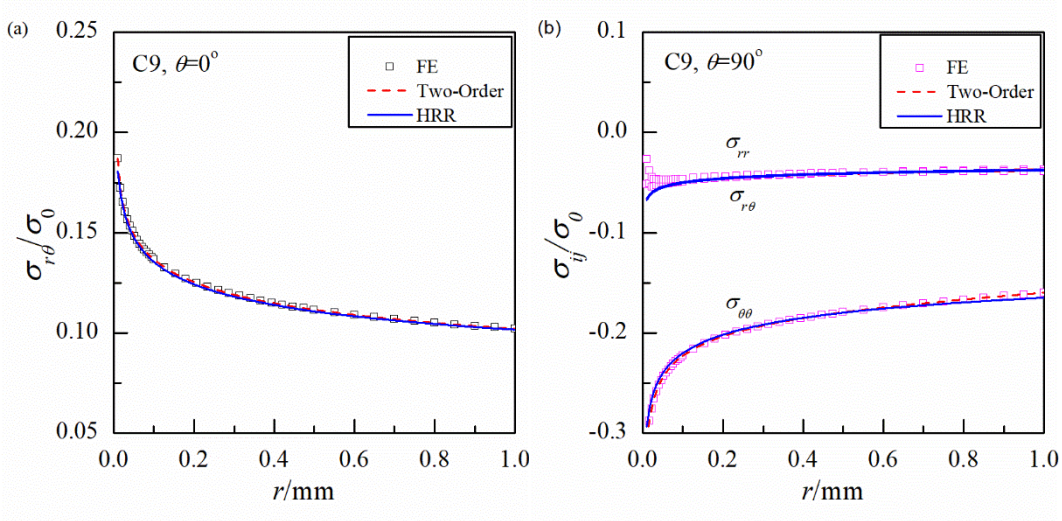

Fig. 19 Comparisons of radial stress distributions for C9 between FE, HRR and two-order term solutions along (a) 0° and (b) 90°

4.3.4 Variation of second order term with creep time

As shown in previous Sections, the stress field is influenced by the material mismatch greatly. To investigate the influence of material mismatch, the $\hat{A}_2(t)$ under various mismatch factors are illustrated in Fig. 20. Note that these data are obtained at r=1 mm along 90° with the shearing stress component. Clearly, it can be seen that variations of $\hat{A}_2(t)$ with normalized creep time and it finds: (1) $\hat{A}_2(t)$ is dependent on creep time if the redistribution time is not reached and the value of $\hat{A}_2(t)$ presents to be nearly a constant if the extensive creep is approached; (2) the $\hat{A}_2(t)$ level is generally higher than the homogeneous case and (3) the overmatch condition presents the higher constraint level than the other cases and the undermatch condition generally shows the lower constraint level than the general evenmatch conditions. From those solutions, it can be deduced that the stress field of mode II creep crack tip is influenced by both general mismatch effect and local mismatch effect.

If one takes the stress field under extensive creep range into consideration, the variations of the $\hat{A}_2(t)$ with normalized distance $\bar{r}$, i.e. $\log\left(r\dot{\varepsilon}_0\sigma_0/C(t)\right)$, are given in Fig. 20. Obviously, the variations of $\hat{A}_2(t)$ along normalized distance away from

the mode II creep crack can be categorized into three kinds of tendencies, which are strongly dependent on the material constants in the position where the crack tip locates. It also illustrates the significance of the effect of the local mismatch effect.

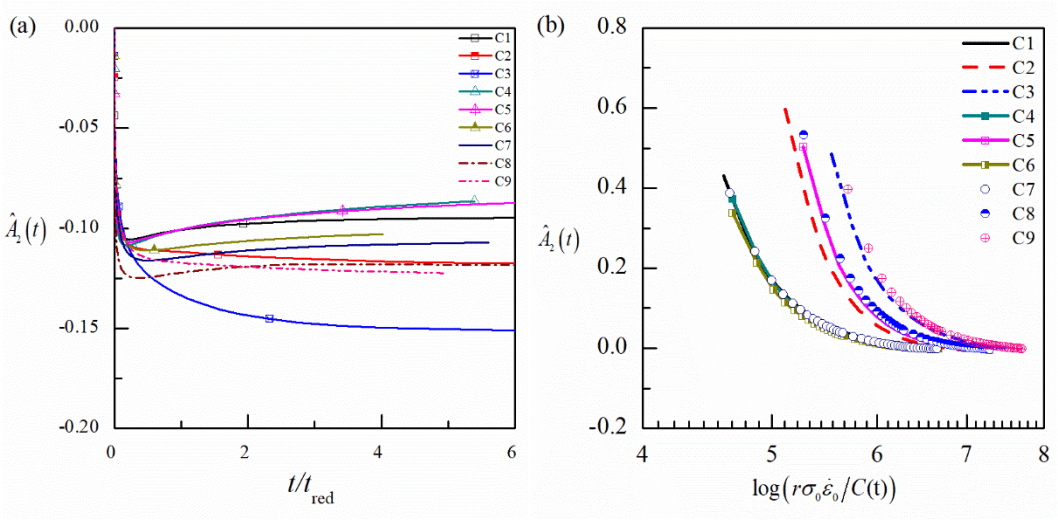

Fig. 20 Variations of the $\hat{A}_2(t)$ under different mismatch factors: (a) variations with creep time; (b) variations with normalized distance

4.4 Influence of creep exponent

Note that the mismatched creep crack tip field under mode II condition given in previous Sections are calculated with the same creep exponent, i.e. n=7. However, the creep exponent can be also different in engineering practices. In order to investigate the influence of creep exponents on the mismatched mode II creep crack tip, three typical creep exponents with the same creep coefficient are adopted and shown in Table 3 which are numbered from C10 to C12. To express the mismatch effect, the mismatch factor is defined as below if the creep exponent is not the same.

$$MF_{\mathrm{w}} = \left(B_{\mathrm{w}}\right)^{-1/n_{\mathrm{w}}} \left(B_{\mathrm{b}}\right)^{1/n_{\mathrm{b}}} \tag{14}$$

$$MF_{\mathrm{HAZ}} = \left(B_{\mathrm{HAZ}}\right)^{-1/n_{\mathrm{w}}} \left(B_{\mathrm{b}}\right)^{1/n_{\mathrm{b}}} \tag{15}$$

Table 3 Material constants used in the comparisons of effect for creep exponent

B_b=B_{HAZ}=B_w	n_w	n_{HAZ}	n_b	MF_W	MF_{HAZ}	ID
3.2E-19	5	7	5	1.0	0.0877	C10
3.2E-19	9	7	9	1.0	3.865	C11
3.2E-19	5	7	9	44.0	3.865	C12

The comparisons of angular stress distributions for C10, C11 and C12 between FE, HRR and Two-Order term solutions at 1 mm are shown in Fig. 21. It should be mentioned that the HRR field is still calculated by Eq. (12). Results show that the FE solutions of C10 are generally higher than the HRR field. The results of C11 present that the FE solutions deviate from the HRR field slightly. However, the results of C12 show that the FE solutions are lower than those of HRR field.

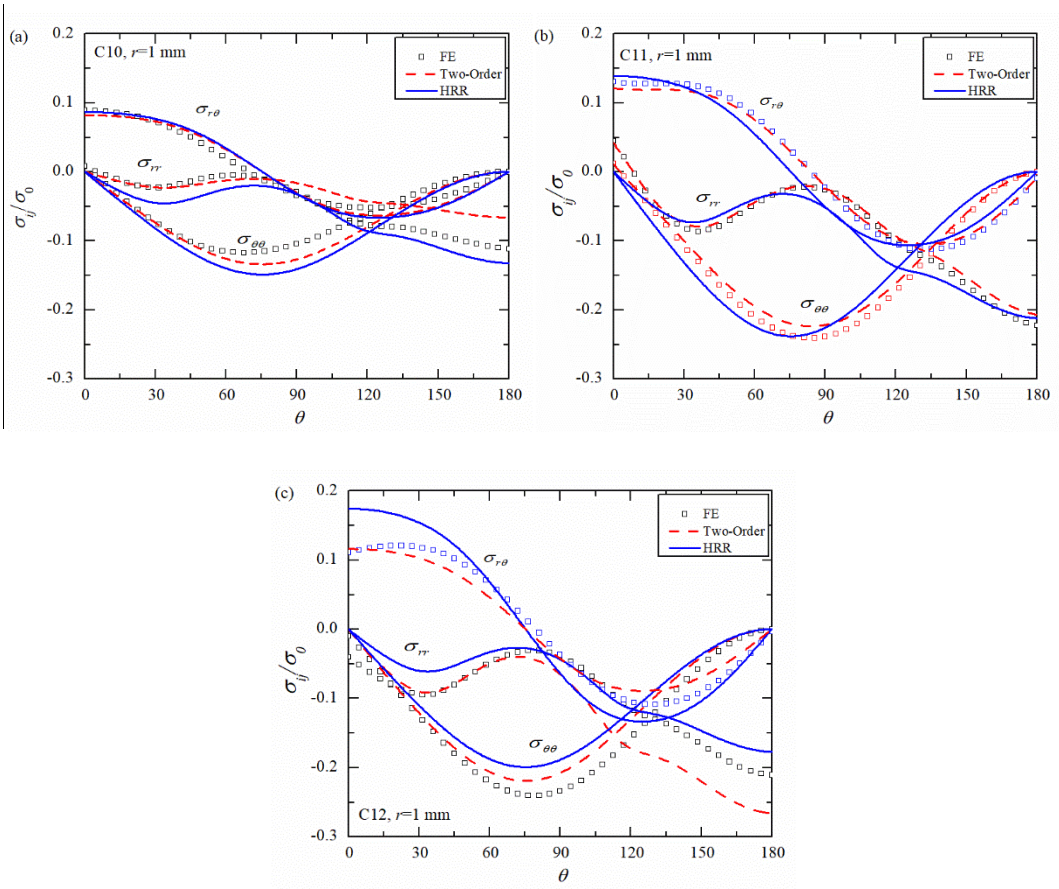

Fig. 21 Comparisons of angular stress distributions for (a) C10, (b) C11 and (c) C12 between FE, HRR and two-order term solutions at r=1 mm

The radial distributions for C10, C11 and C12 along 0° and 90° are shown in Fig. 22, Fig. 23 and Fig. 24, respectively. From Fig. 22, it can be found that there exists the difference between FE solutions and the HRR field and the HRR field is slightly lower than the FE results. For C11, the FE solutions are lower than the HRR field. The discrepancy between HRR field and FE result is also remarkable. Fig. 25 is presented to clarify the difference of the $\hat{A}_2(t)$-term under different creep exponents. It can be found that the $\hat{A}_2(t)$-term for C10 is higher than C11 and C12. The $\hat{A}_2(t)$-term of

C11 is greater than that of C12 if the creep time is less than 4 times of t_{red} and the $\hat{A}_2(t)$ approaches to be close to C12 with the increase of creep time. The $\hat{A}_2(t)$-term is nearly a constant if the extensive creep is reached.

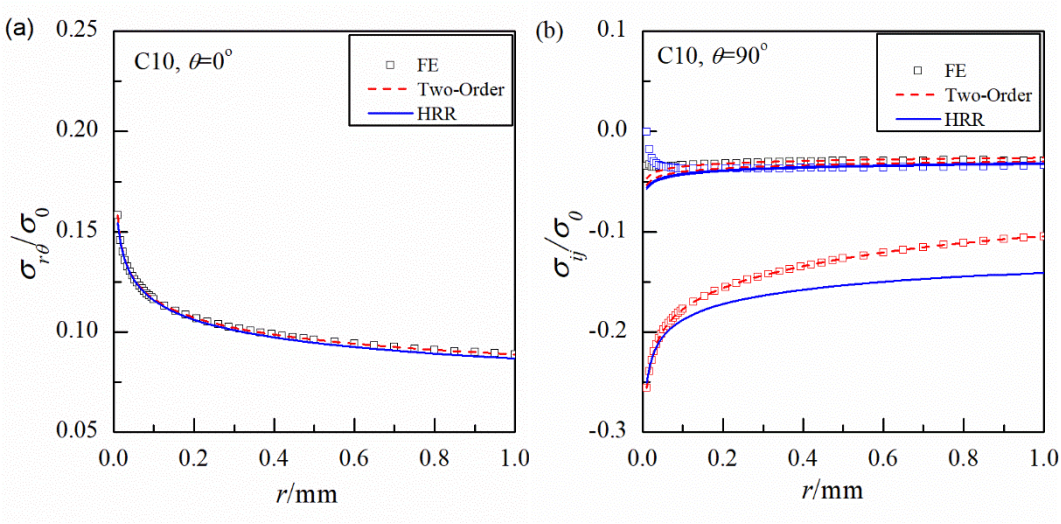

Fig. 22 Comparisons of radial stress distributions for C10 between FE, HRR and Two-Order term solutions along (a) 0° and (b) 90°

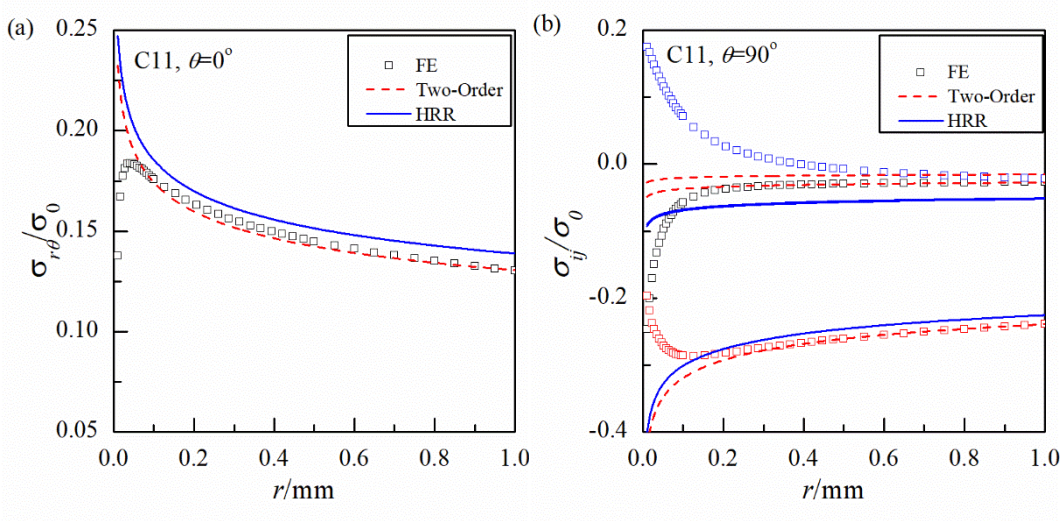

Fig. 23 Comparisons of radial stress distributions for C11 between FE, HRR and two-order term solutions along (a) 0° and (b) 90°

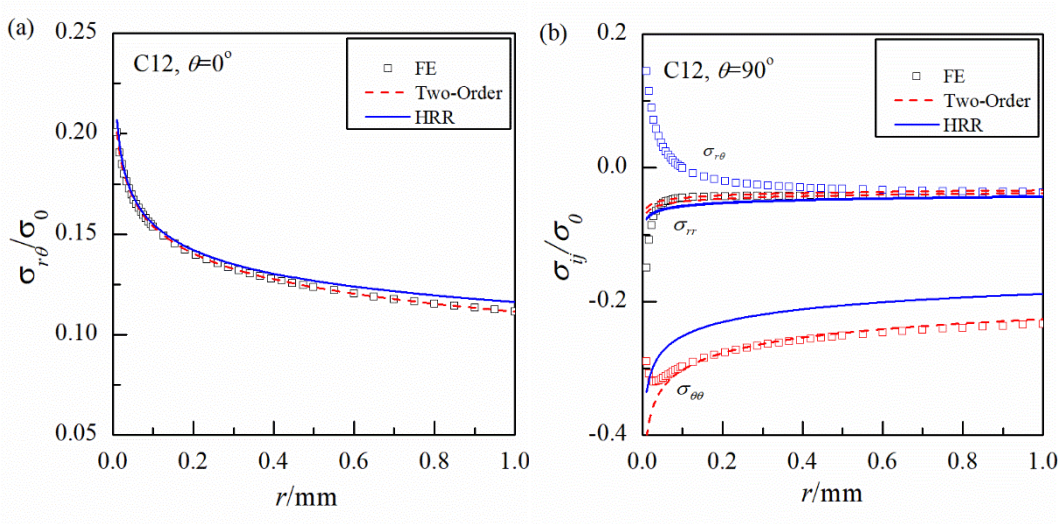

Fig. 24 Comparisons of radial stress distributions for C12 between FE, HRR and two-order term solutions along (a) 0° and (b) 90°

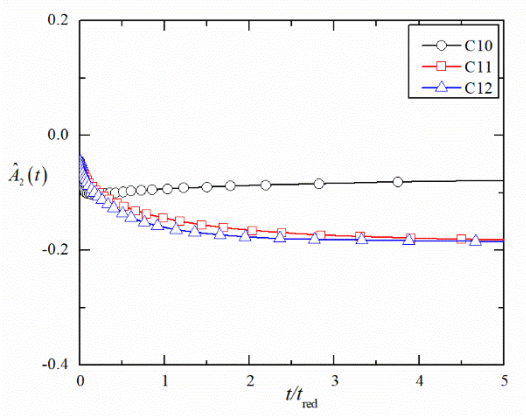

Fig. 25 Variations of the second order term with normalized creep time for C10, C11 and C12

4.5 Influence of HAZ width

In fact, the creep crack tip field is strongly related with the thickness of the HAZ which means that the material mismatch effect could be influenced by the HAZ thickness. From the solutions and comparisons shown in Fig. 26, it can be concluded that the stress field decreases with MF_{HAZ} for the general undermatch condition and this effect can be heightened by the decrease of the HAZ thickness. For the general overmatch condition, the stress field weakens with the rise of MF_{HAZ} as if the HAZ thickness decreases. Similar conclusion can be drawn for the evenmatch condition. However, it should be pointed out that the FE solutions coincide with the higher order

term solutions quite reasonably regardless of the effect of material mismatch.

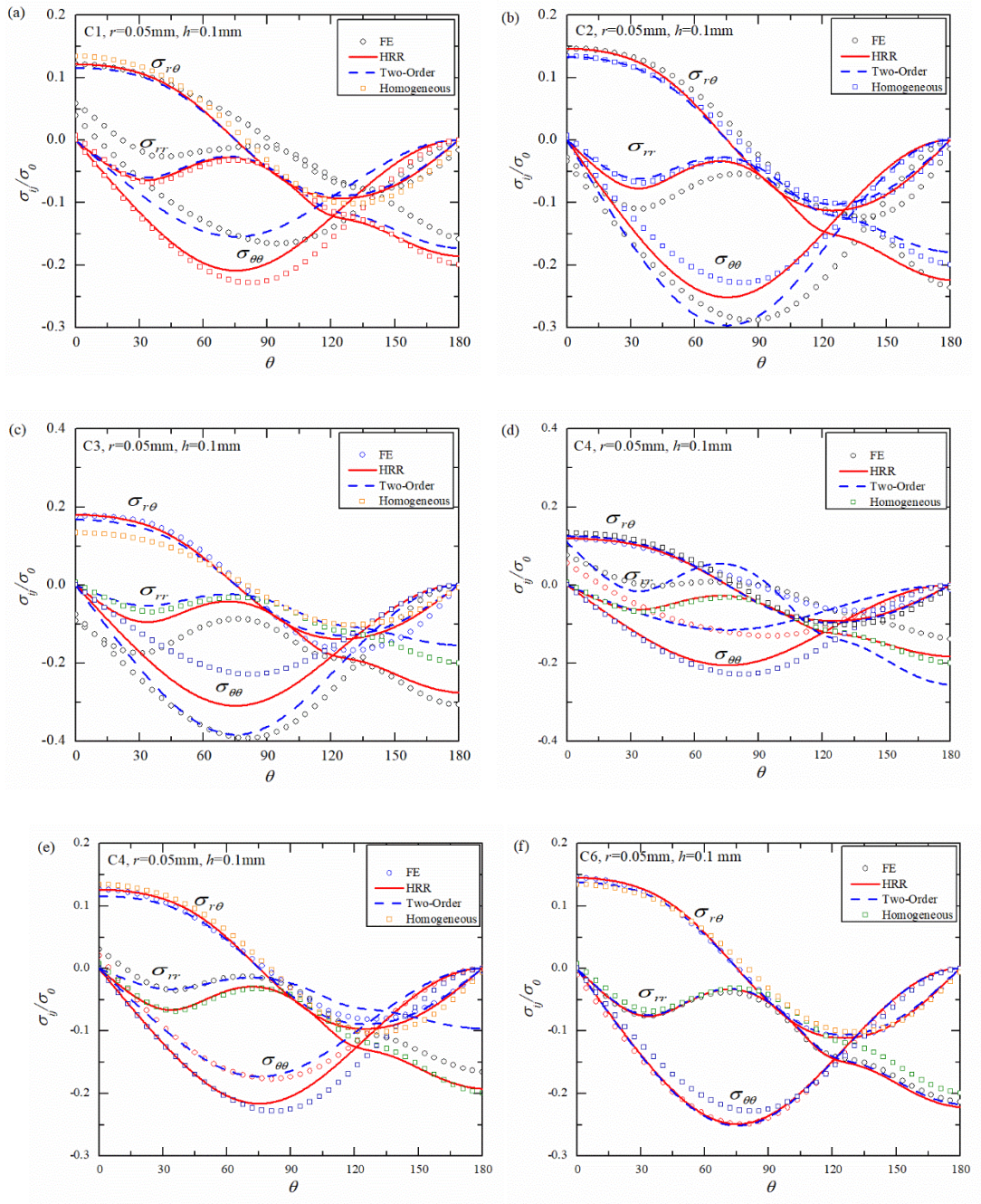

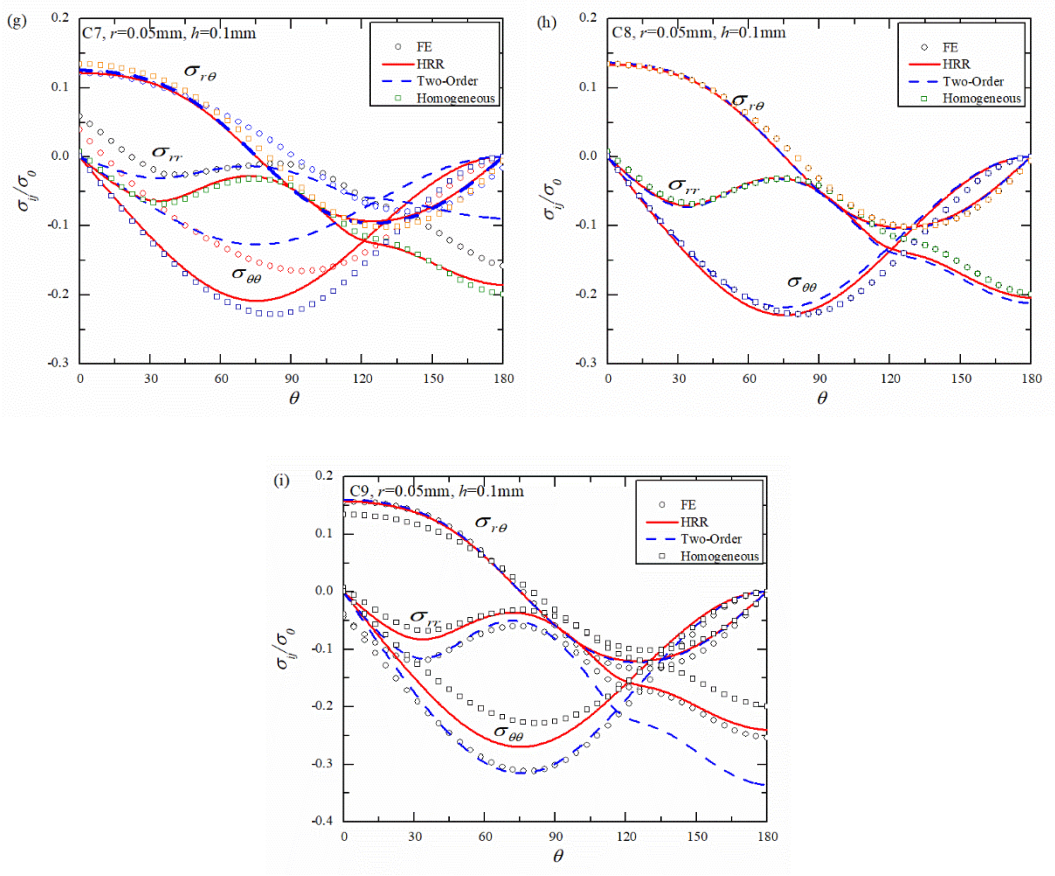

Fig. 26 Comparisons of angular stress distributions between FE, HRR and two-order term solutions at r=0.05mm with h = 0.1 mm: (a) C1; (b) C2; (c) C3; (d) C4; (e) C5; (f) C6; (g) C7; (h) C8; (i) C9

5 Implications of material mismatch effect on mode II creep crack growth

Note that the creep crack growth of mode II creep crack can be predicted by the following relation [49].

$$\dot{a}_0 = \int_0^{r_c} \dot{D}_c \mathrm{d}r \tag{16}$$

where r_c is the size of fracture process zone. For rigorous mode II creep crack, the fracture process zone is ahead of creep crack at the bisector. Herein, one assumes that the stress based damage model is considered to be still valid for the mode II creep crack growth. The form of $\dot{D}_c$ should be provided as [49]

$$\dot{D}_{\mathrm{c}}=\frac{\sigma_{\mathrm{uni}}^{-\chi}\left[\alpha\sigma_{e}+\left(1-\alpha\right)\sigma_{1}\right]^{\chi}}{t_{r}^{0}} \tag{17}$$

where t_r^0 is the creep rupture time which is tested at the uniaxial constant stress σ_{uni}. σ_1 and σ_e are maximum principle stress and equivalent stress, respectively. α and χ are two constants. For α, the range of it varies between 0 and 1. For χ, the values is generally considered to be less than creep exponent *n*.

Considering that the tangential stress and equivalent stress of mode II creep crack under mismatching condition which is given as:

$$\frac{\hat{\sigma}_{22}\left(r,\theta,t\right)}{\sigma_{0}^{\mathrm{tip}}}=\hat{A}_{1}\left(t\right)\overline{r}^{s_1}\tilde{\sigma}_{22}^{(1)}\left(\theta\right)+\hat{A}_{2}\left(t\right)\overline{r}^{s_2}\tilde{\sigma}_{22}^{(2)}\left(\theta\right) \tag{18}$$

$$\frac{\hat{\sigma}_{\mathrm{e}}\left(r,\theta,t\right)}{\sigma_{0}^{\mathrm{tip}}}=\left[\hat{A}_{1}^{2}\left(t\right)\overline{r}^{2s_1}\left(\tilde{\sigma}_{e}^{(11)}\left(\theta\right)\right)^{2}+2\hat{A}_{1}\left(t\right)\hat{A}_{2}\left(t\right)\overline{r}^{s_2-s_1}\tilde{\sigma}_{e}^{(12)}\left(\theta\right)\right]^{1/2} \tag{19}$$

where s_1, s_2 are the stress components of different order terms which have been defined previously. Based on the assumption of [49], the principal stress σ_1 is replaced by tangential stress σ_{22}. Substituting Eqs. (18)-(19) into Eqs. (16) and (17), $\dot{D}_{\mathrm{c}}$ and $\dot{a}$ is given as below:

$$\dot{a}=\int_{0}^{r_{\mathrm{c}}}\hat{A}_{1}^{\chi}\left(t\right)r^{vs_1}\left[\alpha\tilde{\sigma}_{\mathrm{e}}^{(1)}+\left(1-\alpha\right)\tilde{\sigma}_{22}^{(1)}\right]^{\chi}\left\{1+\beta\right\}^{\chi}\mathrm{d}r \tag{20}$$

where β is expressed as following form.

$$\beta=\frac{\left(1-\alpha\right)\hat{A}_{2}\left(t\right)r^{s_2-s_1}\tilde{\sigma}_{22}^{(2)}}{\hat{A}_{1}\left(t\right)\left[\alpha\tilde{\sigma}_{\mathrm{e}}^{(11)}+\left(1-\alpha\right)\tilde{\sigma}_{22}^{(1)}\right]} \tag{21}$$

In integrating form, the creep crack growth rate is written as following.

$$\dot{a}=\frac{n+1}{n+1-v}\hat{A}_{1}^{\chi}\left(t\right)\left[\alpha\tilde{\sigma}_{\mathrm{e}}^{(1)}+\left(1-\alpha\right)\tilde{\sigma}_{22}^{(1)}\right]^{\chi}\left\{1+\beta\right\}^{\chi}\int_{0}^{r_{\mathrm{c}}}r^{-\chi s_1}\mathrm{d}r \tag{22}$$

For a creep crack, the constraint parameter $\hat{A}_2\left(t\right)$ should be a constant under steady state, which does not depend on the radial distance r. Under this condition, the term $\left\{1+\beta\right\}^{\chi}$ can be also considered to be a constant term. Thus, the creep crack growth

considering material mismatch is written as below:

$$\dot{a}=\frac{n+1}{n+1-v}\hat{A}_1^{\chi}\left(t\right)\left[\alpha\tilde{\sigma}_{\mathrm{e}}^{(1)}+\left(1-\alpha\right)\tilde{\sigma}_{22}^{(1)}\right]^{\chi}\left\{1+\beta^{*}\right\}^{\chi}r_{\mathrm{c}}^{\frac{2n+2-\chi}{n+1}} \tag{22}$$

Herein, β^{*} is presented as below:

$$\beta^{*}=\frac{\left(1-\alpha\right)\hat{A}_2^{*}r_{\mathrm{c}}^{s2-s1}\tilde{\sigma}_{22}^{(2)}}{\hat{A}_1^{*}\left[\alpha\tilde{\sigma}_{\mathrm{e}}^{(11)}+\left(1-\alpha\right)\tilde{\sigma}_{22}^{(1)}\right]} \tag{23}$$

where $\hat{A}_1^{*}$ and $\hat{A}_2^{*}$ are the first order term and second order term under extensive creep, respectively.

Note that if effect of higher order term is not considered, Eq. (20) is given as below if one let $\hat{A}_2\left(t\right)$ to be identical to 0.

$$\dot{a}_0=\int_0^{r_{\mathrm{c}}}\hat{A}_1^{\chi}\left(t\right)r^{\chi s_1}\left[\alpha\tilde{\sigma}_{\mathrm{e}}^{(1)}+\left(1-\alpha\right)\tilde{\sigma}_{22}^{(1)}\right]^{\chi}\mathrm{d}r \tag{24}$$

where $\dot{a}_0$ represents the creep crack growth rate without considering higher order term. Hence, the ratio of $\dot{a}/\dot{a}_0$ is given as below, which reflects the effect of higher order term effect.

$$g^{*}=\frac{\dot{a}}{\dot{a}_0}=\left\{1+\beta^{*}\right\}^{\chi} \tag{25}$$

Herein, the modification coefficient is written as

$$g^{*}=\left\{1+\beta_{\mathrm{m}}+\beta_{\mathrm{g}}\right\}^{\chi} \tag{26}$$

in which β_{m} and β_{g} are the coefficients depending on material mismatch and specimen geometry, and the expressions can be given as following.

$$\beta_{\mathrm{m}}=\frac{\left(1-\alpha\right)\hat{A}_{2m}\left(t\right)r_{\mathrm{c}}^{s2-s1}\tilde{\sigma}_{22}^{(2)}}{\hat{A}_1\left(t\right)\left[\alpha\tilde{\sigma}_{\mathrm{e}}^{(11)}+\left(1-\alpha\right)\tilde{\sigma}_{22}^{(1)}\right]} \tag{27}$$

$$\beta_{g}=\frac{\left(1-\alpha\right)\hat{A}_{2g}\left(t\right)r_{\mathrm{c}}^{s2-s1}\tilde{\sigma}_{22}^{(2)}}{\hat{A}_1\left(t\right)\left[\alpha\tilde{\sigma}_{\mathrm{e}}^{(11)}+\left(1-\alpha\right)\tilde{\sigma}_{22}^{(1)}\right]} \tag{28}$$

in which $\hat{A}_{2m}\left(t\right)$ and $\hat{A}_{2g}\left(t\right)$ represent the second order terms which reflect the material mismatch contribution and geometry contribution, respectively. It should be emphasized that the form of Eq. (26) is based on the assumption that the material

constraint effect and geometry constraint can be separated independently. The validation for separation of β_{m} and β_{g} is another topic which will not be discussed in this paper.

If the geometry effect is not taken into consideration, g^* only contains the material mismatch effect. Thereafter, g^* is expressed as

$$g^* = \{1+\beta_{\mathrm{m}}\}^{\nu} \tag{29}$$

Based on Eq. (29), the creep crack grow length is defined as Δa which is computed as following.

$$\Delta a = \dot{a}_0 \cdot g^* \cdot t \tag{30}$$

If one substitutes Eq. (29) into the creep fracture toughness, the creep fracture toughness is given as below.

$$K^{\mathrm{c}}_{\mathrm{mat}} = \left[E\left(\Delta a / b g^*\right)^{1/q} t^{1-1/q} \right]^{1/2} \tag{31}$$

in which parameters b and q are constants depending on creep crack growth rate, i.e.

$$\dot{a}_0 = b\left(C^*\right)^q \tag{32}$$

The discussions on determination of b and q can be found in [29].

Based on Eq. (31), the effect of material mismatch on the creep toughness can be obtained smoothly. It indicates that the material mismatch effect on creep toughness can be obtained through computations from Eq. (16) to (31).

6 Concluding Remarks

The mismatch effect on the mode II creep crack tip field is investigated in this paper. Based on the numerical calculations and theoretical analysis, the following conclusions are obtained.

1) $C(t)$-integral of mismatched mode II creep crack is found to be influenced by the material mismatch greatly. It is found that C^*-integral decreases with the increase

of MF_{HAZ} regardless of MF_{W} and HAZ width. C^*-integral also decreases with the rise of MF_{W} for a fixed MF_{HAZ}. C^*-integral is also affected by the HAZ width and the effect of the HAZ width on C^*-integral is dependent on the range of mismatch factor.

2) The stress field of the mode II creep crack is found to be influenced by the material mismatch effect greatly. These cases with lower creep coefficient present to have the higher stress components. Results show that the first order analytical stress field can be estimated by the HRR field with the material constants where the crack tip locates. There exists the difference between the mismatched creep crack tip field and the analytical HRR field which reveals that the high order term is needed to characterize the material mismatch effect.

3) The two-order termed asymptotic solutions for mode II creep crack is presented. A high order term $\hat{A}_2(t)$ is proposed, which can take the mismatch effect as well as the geometry effect on the high order term solutions into considerations. Three typical mismatch conditions are presented which show that the effect of local mismatch plays a significant role in the material mismatch constraint effect.

4) The creep exponent is also found to be important on the mismatch creep crack tip field under mode II loading. Different combinations of the creep exponent will lead to different variation tendencies as well as the high order term solutions. In general, the lower creep exponent for base and weld metal with a higher creep exponent for HAZ material will lead to the higher level of $\hat{A}_2(t)$.

5) As for the influence of the HAZ thickness on the mismatched creep crack tip field, the stress field presents to become lower with the decrease of creep exponent regardless of the general overmatch, general undermatch and general evenmatch condition. A theoretical formula is presented to show the implication of material mismatch effect on creep crack growth under mode II condition based on stress damage model.

It should be mentioned that the mismatch effect can be caused by many factors.

The solutions presented in this paper could further promote the understanding of the mismatch effect on the creep crack tip field under mode II loading.

Acknowledgement

The authors acknowledge the supports from the Beijing Natural Science Foundation (2204074), the National Natural Science Foundation of China (11902009), and the Scientific Research Common Program of Beijing Municipal Commission of Education (KM202010005034). The authors would like to thank Prof. Yuh-Jin Chao for the helpful discussion on the content of this paper.

Appendix A Stress distributions of the two order

For the mode II creep crack in a power-law creeping materials, the first order asymptotic solution still satisfies the HRR singularity, i.e. $s_1 = -1/(n+1)$ in Eq. (4), and the angular distributions are presented in Fig. A1 (a). With the shooting method similar to that presented in [44], the second order angular distributions for n=7 for creeping material are presented in Fig. (b) with $s_2 = 0.3209$.

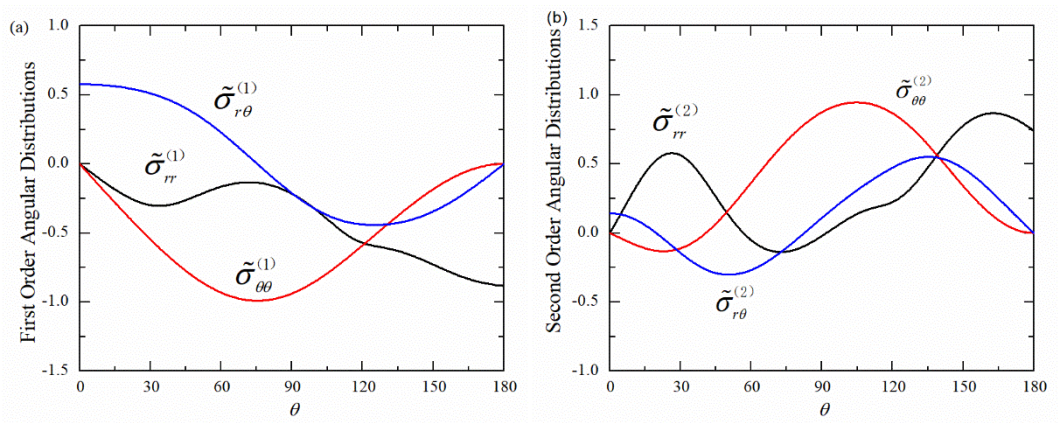

Fig. A1 Angular distributions functions of different orders for n=7: (a) the first order; (b) the second order

References

[1] Gallo P, Berto F, Glinka G. 2016, Analysis of creep stresses and strains around sharp and blunt V-notches. Theoretical and Applied Fracture Mechanics 85, 435-446.

[2] Gallo P, Berto F, Glinka G. 2016. Generalized approach to estimation of strains and stresses at blunt Vnotches under non-localized creep. Fatigue & Fracture of Engineering Materials & Structures 39(3), 292-306.

[3] Hyde, T., Sun, W., Williams, J., 2003. Creep analysis of pressurized circumferential pipe weldments—a review. The Journal of Strain Analysis for Engineering Design 38, 1-27.

[4] Tabuchi, M., Watanabe, T., Kubo, K., Matsui, M., Kinugawa, J., Abe, F., 2001. Creep crack growth behavior in the HAZ of weldments of W containing high Cr steel. International Journal of Pressure Vessels and Piping 78, 779-784.

[5] Budden, P., Curbishley, I., 2000. Assessment of creep crack growth in dissimilar metal welds. Nuclear Engineering and Design 197, 13-23.

[6] Saber, M., Sun, W., Hyde, T., 2016. Numerical study of the effects of crack location on creep crack growth in weldment. Engineering Fracture Mechanics 154, 72-82.

[7] Dongquan Wu, Hongyang Jing, Lianyong Xu, Lei Zhao, Yongdian Han, Theoretical and numerical analysis of creep crack initiation combined with primary and secondary stresses, Theoretical and Applied Fracture Mechanics, 2018, 95, 143-154.

[8] Zerbst, U., Ainsworth, R.A., Beier, H.T., Pisarski, H., Zhang, Z.L., Nikbin, K., Nitschke-Pagel, T., Münstermann, S., Kucharczyk, P., Klingbeil, D., 2014. Review on fracture and crack propagation in weldments-A fracture mechanics perspective. Engineering Fracture Mechanics 132, 200-276.

[9] Lucie Malíková, Václav Veselý, Influence of the elastic mismatch on crack propagation in a silicate-based composite, Theoretical and Applied Fracture Mechanics, 2017, 91, 25-30.

[10] Mei, H., Pang, Y., Huang, R., 2007. Influence of interfacial delamination on channel cracking of elastic thin films. International Journal of Fracture 148, 331-342.

[11] Romeo, A., Ballarini, R., 1994. The influence of elastic mismatch on the size of the plastic zone of a crack terminating at a brittle-ductile interface. International Journal of Fracture 65, 183-196.

[12] Schmauder, S., Müller, W., 1991. On the influence of elastic mismatch on stress intensity factors of cracks perpendicular to a bimaterial interface. International Journal of Fracture 51, R21-R27.

[13] Betegón, C., Peñuelas, I., 2006. A constraint based parameter for quantifying the crack tip stress fields in welded joints. Engineering fracture mechanics 73, 1865-1877.

[14] Burstow, M.C., Howard, I.C., Ainsworth, R.A., 1998. The influence of constraint on crack tip stress fields in strength mismatched welded joints. Journal of the Mechanics and Physics of Solids 46, 845-872.

[15] Kumar, S., Khan, I.A., Bhasin, V., Singh, R.K., 2014. Characterization of crack tip stresses in plane-strain fracture specimens having weld center crack. International Journal of Solids and Structures 51, 1464-1474.

[16] Zhang, Z.L., Hauge, M., Thaulow, C., 1996. Two-parameter characterization of the near-tip stress fields for a bi-material elastic-plastic interface crack. International Journal of Fracture

79, 65-83.
[17] Duan C, Zhang S. 2020, Two-parameter J-A estimation for weld centerline cracks of welded SE(T) specimen under tensile loading. Theoretical and Applied Fracture Mechanics, 107, 102435.
[18] S.T. Tu, 2002, Creep behavior of crack near bi-material interface characterized by integral parameters, Theoretical and Applied Fracture Mechanics, 38, (2), 203-209.
[19] Chen, G., Wang, G.Z., Xuan, F.Z., Tu, S.T., 2014. Mismatch effect in creep properties on creep crack growth behavior in welded joints. Materials & Design 63, 600-608.
[20] Dai, Y., Liu, D., Liu, Y., 2016. Mismatch constraint effect of creep crack with modified boundary layer model. Journal of Applied Mechanics 83, 031008-031016.
[21] Lai, H.S., Yoon, K.B., 2016. Study on the estimation of high temperature fracture parameter for mismatched weld creep cracks. Engineering Fracture Mechanics 163, 117-129.
[22] Lee, K.H., Kim, Y.J., Yoon, K.B., Nikbin, K., Dean, D., 2010. Quantification of stress redistribution due to mismatch in creep properties in welded branch pipes. Fatigue & Fracture of Engineering Materials & Structures 33, 238-251.
[23] Wenchun Jiang, Yun Luo, Baozhu Zhang, S.-H. Li, X.-F. Xie, Shan-Tung Tu, Characterization of creep constraint effect for brazed joint specimens at crack tip by new constraint parameter As, Theoretical and Applied Fracture Mechanics, 2020, 109, 102707.
[24] Segle, P., Andersson, P., Samuelson, L.Å., 2000. Numerical investigation of creep crack growth in cross-weld CT specimens. Part I: influence of mismatch in creep deformation properties and notch tip location. Fatigue & Fracture of Engineering Materials & Structures 23, 521-531.
[25] Kim, Y.-J., Schwalbe, K.-H., 2001. Mismatch effect on plastic yield loads in idealised weldments: I. Weld centre cracks. Engineering Fracture Mechanics 68, 163-182.
[26] Lee, H., Kim, Y.-J., 2001. Interfacial crack-tip constraints and J-integrals in plastically mismatched bi-materials. Engineering Fracture Mechanics 68, 1013-1031.
[27] Biner, S.B., 1997. A numerical analysis of time dependent stress fields ahead of stationary interface cracks at creep regime—Part II. Interface cracks in layered materials. Engineering Fracture Mechanics 56, 657-674.
[28] Xuan, F.-Z., Tu, S.-T., Wang, Z., 2004. C* estimation for cracks in mismatched welds and finite element validation. International Journal of Fracture 126, 267-280.
[29] Davies, C.M., Dean, D.W., Nikbin, K.M., O'Dowd, N.P., 2007. Interpretation of creep crack initiation and growth data for weldments. Engineering Fracture Mechanics 74, 882-897.
[30] Assire, A., Michel, B., Raous, M., 2001. Creep crack initiation and creep crack growth assessments in welded structures. Nuclear Engineering and Design 206, 45-56.
[31] Dogan, B., Petrovski, B., 2001. Creep crack growth of high temperature weldments. International Journal of Pressure Vessels and Piping 78, 795-805.
[32] Sugiura, R., Yokobori, A.T., Suzuki, K., Tabuchi, M., 2010. Characterization of incubation time on creep crack growth for weldments of P92. Engineering Fracture Mechanics 77, 3053-3065.
[33] Yatomi, M., Tabuchi, M., 2010. Issues relating to numerical modelling of creep crack growth. Engineering Fracture Mechanics 77, 3043-3052.
[34] Poquillon, D., Cabrillat, M., Pineau, A., 1999. Mode II creep crack initiation in 316 LN stainless steel: experiments and modelling. Materials at high temperatures 16, 99-107.
[35] Brockenbrough, J., Shih, C., Suresh, S., 1991. Transient crack-tip fields for mixed-mode power law creep. International Journal of Fracture 49, 177-202.

[36] Dai, Y., Liu, Y., Chao, Y.J., 2017. Higher order asymptotic analysis of crack tip fields under mode II creeping conditions. International Journal of Solids and Structures, 125, 89-107.

[37] Dai, Yanwei, Yinghua Liu, and Yuh J. Chao. 2018. Mismatch effect on the mode II type crack tip field in power-law creeping materials. In ASME 2018 Pressure Vessels and Piping Conference.

[38] Norton, F.H., 1929. The creep of steel at high temperatures. McGraw-Hill Book Company, Incorporated.

[39] Symington, M.F., Shih, C.F., Ortiz, M., 1988. Tables of plane strain mixed-mode plastic crack tip fields. Brown University Division of Engineering.

[40] Bassani, J., McClintock, F., 1981. Creep relaxation of stress around a crack tip. International Journal of Solids and Structures 17, 479-492.

[41] Ayatollahi, M., Pavier, M., Smith, D., 1998. Determination of T-stress from finite element analysis for mode I and mixed mode I/II loading. International Journal of Fracture 91, 283-298.

[42] Roy, Y., Narasimhan, R., Arora, P., 1999. An experimental investigation of constraint effects on mixed mode fracture initiation in a ductile aluminium alloy. Acta materialia 47, 1587-1596.

[43] Dai, Yanwei, Yinghua Liu, Fei Qin, Guian Qian, and Yuh J. Chao. 2019. C(t) Dominance of the Mixed I/II Creep Crack: Part I. Transient Creep. Theoretical and Applied Fracture Mechanics 103: 102314.

[44] Dai, Yanwei, Yinghua Liu, Fei Qin, Yuh J. Chao, and Guian Qian. 2020. C(t) Dominance of the Mixed I/II Creep Crack: Part II. Extensive Creep. Theoretical and Applied Fracture Mechanics 106: 102489.

[45] Han, J.J., Kim, Y.J., Jerng, D., Nikbin, K., Dean, D., 2015. Quantification of creep stresses within HAZ in welded branch junctions. Fatigue & Fracture of Engineering Materials & Structures 38, 113-124.

[46] Riedel, H., 1987. Fracture at high temperatures. Springer.

[47] Yang, S., Chao, Y., Sutton, M., 1993. Higher order asymptotic crack tip fields in a power-law hardening material. Engineering Fracture Mechanics 45, 1-20.

[48] Chao, Y.J., Yang, S., 1996. Higher order crack tip fields and its implication for fracture of solids under mode II conditions. Engineering Fracture Mechanics 55, 777-794.

[49] Budden, P. J., Ainsworth R. A., 1999. The effect of constraint on creep fracture assessments. International Journal of Fracture 97(1-4): 237-247.

Table captions

Figure captions